SERI/SP-253-3212
DE89000811

March 1988

Internal Film Receiver Systems Assessment Study

J. V. Anderson

SERI

Solar Energy Research Institute
A Division of Midwest Research Institute
1617 Cole Boulevard
Golden, Colorado 80401-3393

Operated for the
U.S. Department of Energy
under Contract No. DE-AC02-83CH10093

SERI/SP-253-3212
UC Category: 236
DE89000811

Internal Film Receiver Systems Assessment Study

J. V. Anderson

May 1988

Prepared under Task No. ST812831

Solar Energy Research Institute
A Division of Midwest Research Institute

1617 Cole Boulevard
Golden, Colorado 80401-3393

Prepared for the
U.S. Department of Energy
Contract No. DE-AC02-83CH10093

NOTICE

This report was prepared as an account of work sponsored by an agency of the United States government. Neither the United States government nor any agency thereof, nor any of their employees, makes any warranty, express or implied, or assumes any legal liability or responsibility for the accuracy, completeness, or usefulness of any information, apparatus, product, or process disclosed, or represents that its use would not infringe privately owned rights. Reference herein to any specific commercial product, process, or service by trade name, trademark, manufacturer, or otherwise does not necessarily constitute or imply its endorsement, recommendation, or favoring by the United States government or any agency thereof. The views and opinions of authors expressed herein do not necessarily state or reflect those of the United States government or any agency thereof.

Printed in the United States of America
Available from:
National Technical Information Service
U.S. Department of Commerce
5285 Port Royal Road
Springfield, VA 22161

Price: Microfiche A01
Printed Copy A04

Codes are used for pricing all publications. The code is determined by the number of pages in the publication. Information pertaining to the pricing codes can be found in the current issue of the following publications which are generally available in most libraries: *Energy Research Abstracts (ERA)*; *Government Reports Announcements* and Index (*GRA* and I); *Scientific and Technical Abstract Reports (STAR)*; and publication NTIS-PR-360 available from NTIS at the above address.

PREFACE

The research and development described in this document was conducted within the U.S. Department of Energy's Solar Thermal Technology Program. The goal of this program is to advance the engineering and scientific understanding of solar thermal technology and to establish the technology base from which private industry can develop solar thermal power production options for introduction into the competitive energy market.

Solar thermal technology concentrates the solar flux using tracking mirrors or lenses onto a receiver where the solar energy is absorbed as heat and converted into electricity or incorporated into products as process heat. The two primary solar thermal technologies, central receivers and distributed receivers, employ various point and line-focus optics to concentrate sunlight. Current central receiver systems use fields of heliostats (two-axes tracking mirrors) to focus the sun's radiant energy onto a single, tower-mounted receiver. Point focus concentrators up to 17 meters in diameter track the sun in two axes and use parabolic dish mirrors or Fresnel lenses to focus radiant energy onto a receiver. Troughs and bowls are line-focus tracking reflectors that concentrate sunlight onto receiver tubes along their focal lines. Concentrating collector modules can be used alone or in a multimodule system. The concentrated radiant energy absorbed by the solar thermal receiver is transported to the conversion process by a circulating working fluid. Receiver temperatures range from 100°C in low-temperature troughs to over 1500°C in dish and central receiver systems.

The Solar Thermal Technology Program is directing efforts to advance and improve each system concept through solar thermal materials, components, and subsystems research and development and by testing and evaluation. These efforts are carried out with the technical direction of DOE and its network of field laboratories that works with private industry. Together they have established a comprehensive, goal-directed program to improve performance and provide technically proven options for eventual incorporation into the Nation's energy supply.

To successfully contribute to an adequate energy supply at reasonable cost, solar thermal energy must be economically competitive with a variety of other energy sources. The Solar Thermal Technology Program has developed components and system-level performance targets as quantitative program goals. These targets are used in planning research and development activities, measuring progress, assessing alternative technology options, and developing optimal components. These targets will be pursued vigorously to ensure a successful program.

The internal film receiver (IFR) is an innovative receiver concept that was proposed as part of the class of film-type receivers, which includes the direct absorption receiver (DAR). This report documents a preliminary effort to define the economic and technical potential of the IFR concept relative to the more conventional salt-in-tube receiver and to the DAR. The IFR is important to the Solar Thermal Technology Program because although it does not have nearly the same potential for cost and performance improvement as the DAR, it does take advantage of the high flowing-film heat transfer coefficients with-

out exposing the working fluid to the atmosphere. Should research efforts on the DAR uncover undesirable behavior related to the exposure of the hot salt to the atmosphere (e.g., salt blow-off or contamination) or more general problems with our current concept of the DAR (e.g., failure to find a stable dopant), then these attributes could cause the IFR to become the flagship in advanced receiver research and development efforts.

John V. Anderson

Approved For

SOLAR ENERGY RESEARCH INSTITUTE

L. M. Murphy, Manager
Thermal Systems Research Branch

for G Groff
Gerald C. Groff, Director
Solar Heat Research Division

TABLE OF CONTENTS

		Page
1.0	Introduction and Summary	1
2.0	Methodology and Results	4
3.0	Conclusions	9
4.0	References	10
Appendix A	Final Report on the IFR Configuration Study from SPECO, Inc	11
Appendix B	Tables of Calculations	57
Distribution List		61

LIST OF FIGURES

1-1	IFR Configuration	1
1-2	Comparison of LECs for Salt-in-Tube, DAR, and IFR Systems	3

LIST OF TABLES

2-1	Receiver Performance Parameters	6
2-2	System Performance Comparison of Annual Energy Values	6
2-3	Plant Capital Cost	7
2-4	Levelized Energy Cost Analysis	8
B-1	Receiver Component Cost Analysis	57
B-2	Receiver Subsystem Cost Analysis	59
B-3	IFR Losses and Annual Performance	60

1.0 INTRODUCTION AND SUMMARY

This report documents SERI's Internal Film Receiver (IFR) system assessment effort. The objective of this effort was to develop the IFR concept to the point where it could reasonably be compared to systems with conventional (tube-type) receivers and to systems with other advanced receivers, such as the direct absorption receiver (DAR) [1]. This report documents that comparison. The receiver configuration work for this effort was performed by SPECO, Inc., under contract to SERI. SPECO's final report is included as Appendix A to this document.

Tibor Buna of SPECO first proposed the IFR concept. It evolved as a variation in the general film receiver category that includes the DAR. The IFR is similar to the DAR in that both use films flowing over nearly vertical plates to absorb the solar energy. However, the working fluid in the DAR is exposed directly to the concentrated radiation, while in the IFR the radiation strikes the outside of the absorber plate and the working fluid flows down the inside. SPECO selected an external receiver with a surround field configuration. This configuration produced an IFR absorber that is an inverted truncated cone that forms a small-angle "funnel" shape, as shown in Figure 1-1. The working fluid (molten nitrate salt) flows from a manifold at the top of this funnel, is heated as it flows down along the absorber panel, and is collected in a "trough" at the bottom (see Appendix A).

The IFR has several advantages over the DAR. The first and, probably, most major is that it isolates the working fluid from the environment. This factor

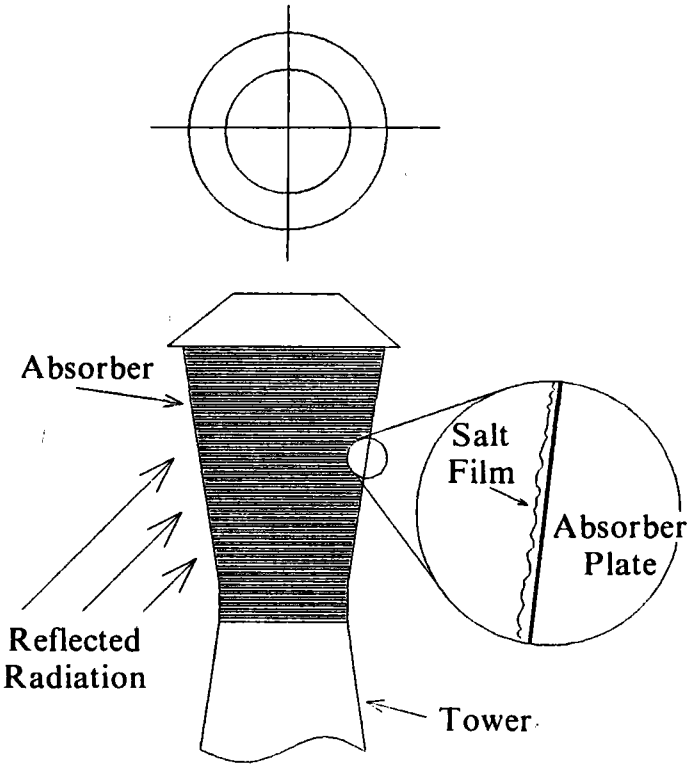

Figure 1-1. IFR Configuration.

could be important if issues such as working fluid blow-off or contamination should prove to be serious problems with the DAR. The second advantage is that the IFR does not require the salt to be doped with optical darkeners. This factor will be a major one if the dopant particles in the DAR should prove to be the source of problems (because of agglomeration or erosion, for example). A third, more minor advantage is that the natural shape of the IFR leaves the absorber pointing down toward the field so that the incident flux is more nearly normal to the surface instead of tilting back away from the field, as in the DAR.

The IFR also has several disadvantages when compared to the DAR. Because the concentrated radiation in the IFR is directly incident on the outer surface of the absorber plate, the IFR absorber plate temperature will always be higher than the DAR plate temperature. This leads to two negative effects. First, the higher plate temperatures lead to higher stresses in the absorber plate. These higher stress levels reduce the allowable fluxes, and ultimately result in a larger receiver. Second, the higher surface temperatures in the IFR cause larger thermal losses and lower receiver efficiency. This effect is described in more detail in Section 2 and Appendix B.

When compared to a conventional salt-in-tube receiver, the IFR has most of the advantages of the DAR but in diminished magnitude. For example, a major factor driving the flux limits for salt-in-tube receivers is the temperature difference between the front and the back walls of the tube. Because the IFR has only one wall, the flux limits will probably be higher than for the salt-in-tube receiver, and the resulting receiver should be smaller and lighter and have lower losses. As with the DAR, the IFR should be simpler to build and operate and require lower pumping power than a salt-in-tube receiver but might not have the same degree of insensitivity to uncertainties in flux levels and gradients as the DAR. Finally, an advantage of the IFR that was not quantified here involves the flexibility to tilt the absorber down towards the field. This could allow a somewhat smaller absorber than accounted for here, and may offer certain advantages in producing a uniform flux profile.

The results of the comparison conducted here are plotted in Figure 1-2. The analysis predicts about a 5% advantage for the base-case IFR system (as proposed by SPECO) over the salt-in-tube receiver system. This advantage compares with about a 15% advantage for the DAR system. Of the 5% advantage for the IFR, roughly 3% can be attributed to improvements in performance and 2% to decreases in capital cost. As with the DAR, no credit was claimed for potential reductions in operations and maintenance costs because these costs are impossible to quantify without at least a more formal design and, probably, some operating experience.

Figure 1-2 also shows the sensitivity of the levelized energy cost (LEC) to the allowable fluxes on the IFR. To fully examine the range of possibilities, the average flux on the IFR was varied from the value used for the Pacific Gas and Electric (PG&E) salt-in-tube receiver design to the level achievable on the DAR. As the average flux increases from the value for the salt-in-tube receiver, the IFR absorber area becomes smaller, but because of the increased flux, the temperature of the outer surface also becomes higher. The net result of these two effects is a small decrease in the LEC with increasing flux levels. Because of several fairly intrinsic decreases in capital cost and parasitics, the IFR has a LEC advantage over the salt-in-tube receiver even at

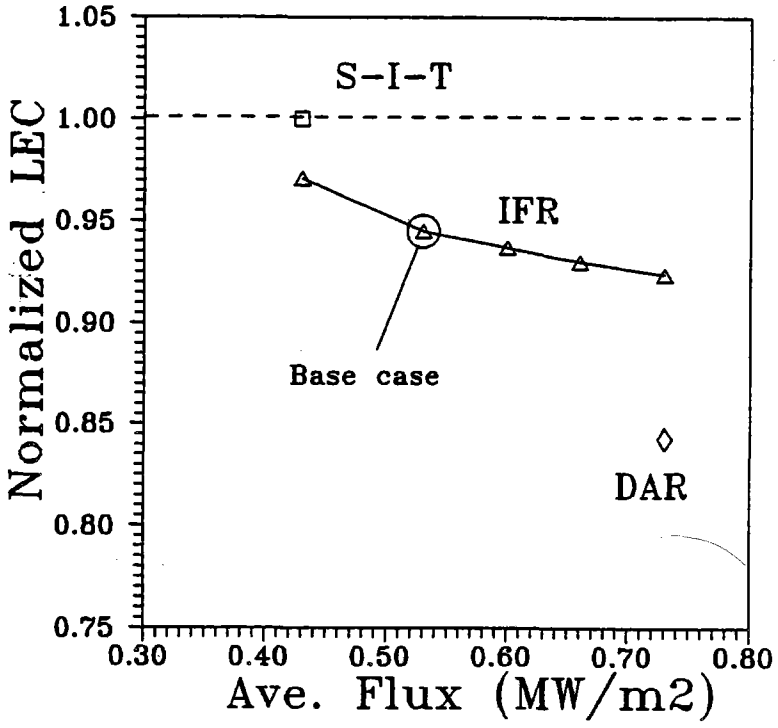

Figure 1-2. Comparison of LECs for Salt-in-Tube, DAR, and IFR Systems.

low fluxes. Similarly, because of the higher external surface temperature and concomittantly higher thermal losses in the IFR, it does not reduce the LEC as much as the DAR, even at high average flux levels.

Based on the potential LEC reductions shown here, the IFR does not appear to have as strong a potential for economic advantage as the DAR. However, the IFR does show some economic potential over the salt-in-tube receiver, and it does avoid some of the potential technical problems with the DAR. However, without some stronger motivation than is apparent in this study, there does not appear to be any reason to pursue the IFR concept at this time.

2.0 METHODOLOGY AND RESULTS

The comparison between the IFR, the DAR, and the salt-in-tube receiver systems was based on the designs developed by the Pacific Gas and Electric team for the Utility Central Receiver Study [2]. All three receiver concepts were compared in an external surround configuration. The salt-in-tube receiver system was exactly as designed by the PG&E team, and the IFR and DAR were patterned on the PG&E sodium receiver design. The power ratings of all three plants were close to the 100 MWe used in the Utility Study, but the ratings of the IFR and DAR varied slightly because their receiver thermal losses varied from those of the original sodium receiver.

The DAR system was modeled on the PG&E sodium system (same absorber size, field size, and tower height). The base-case IFR absorber size was determined using the average flux (0.53 MW/m^2) chosen by SPECO on the basis of its analysis of the thermal stresses in the absorber plate. This produced an absorber area that was about 20% smaller than the salt-in-tube receiver. By comparison, the DAR was about 40% smaller than the salt-in-tube receiver.

However, because of the uncertainty associated with the allowable flux on the IFR, the sensitivity of the results to this parameter was also investigated over the range from the flux level on the salt-in-tube receiver to that on the DAR. Several interesting effects occur as the flux on the IFR is changed. First of all, as the flux increases from the salt-in-tube receiver level, the absorber becomes smaller. However, because of the increased flux, the temperature of the outer surface increases. Although the decrease in area tends to decrease the thermal losses, the increase in temperature increases them. As shown in Figure 1-2, the combination produces a slight trend toward lower losses (and lower LEC) with higher fluxes.

Besides the change in thermal losses, there is another effect associated with changes in the absorber size. As the allowable flux levels decrease and the absorber size increases, the fraction of the radiation reflected from the field that misses the absorber (the spillage) decreases. There is no particularly good way to account for the decrease in spillage with larger absorbers in a brief analysis such as this. Fortunately, the spillage on the (small) high-flux DAR receiver is already fairly low (2.7%). Note that the effect of a more detailed analysis of the spillage would probably be to slightly improve the performance of the IFR at lower flux levels, which would further "flatten" the curve shown in Figure 1-2.

The tower height and the field size for the IFR and DAR were both assumed to be the same as the PG&E sodium system. The components that are downstream from the receiver (e.g., storage, EPGS) were the same for all three plants and were assumed identical to those designed by PG&E for the salt-in-tube receiver system.

The thermal losses for the DAR and IFR were scaled directly from the losses for the salt-in-tube receiver, based on the fundamental characteristics of the heat-loss mechanisms. For example, the losses from radiative emission were assumed to be proportional to

$$A_{abs}\ \varepsilon\ (T_{ave}^4 - T_{amb}^4)\ ,$$

where A_{abs} is the absorber area, ϵ is the absorber surface emittance, T_{ave} is the effective average surface temperature, and T_{amb} is the ambient temperature.

The convective and conductive losses were assumed to be proportional to

$$A_{abs}(T_{ave} - T_{amb}) ,$$

where the approximation is made that the convection coefficient to the air is insensitive to factors such as surface temperature or surface roughness.

The parameters used to scale the receiver losses are shown in Table 2-1. The absorptance and emittance for the salt-in-tube and the IFR receivers are for a Pyromark selective coating and were drawn from the guidelines used for the *Utility Study* designs. The absorptance for the DAR was calculated from the surface reflectance (at the liquid-air interface), an absorptance in the doped salt of approximately 0.8 (in a 1-mm film thickness), and an absorptance for the oxidized stainless steel wall of 0.9*. The DAR emittance was assumed equal to its absorptance.

The average temperature of the outside surface of the IFR absorber was estimated using the temperature profile predicted by SPECO (see Appendix B). This average was calculated using temperatures raised to the fourth power, weighted by the area of the absorber (note that the higher temperatures are at the smaller end of the IFR absorber). It was assumed that the control system would adjust the flow rate so that the SPECO temperature profile would be independent of flux level. This allowed us to use the same average temperature both for all azimuthal positions around the receiver, and for all average flux levels.

The average temperature for the salt-in-tube receiver was determined from the design point emission losses as given by PG&E, and the average temperature for the DAR was calculated as the T^4-weighted average of a linear temperature profile from inlet to outlet.

Once the ratio of the IFR losses relative to the salt-in-tube receiver losses had been determined, these ratios were applied to the annual losses for the salt-in-tube receiver that are reported in the *Utility Study*. The resulting annual receiver losses were then used to determine the IFR efficiency. This receiver efficiency was used with the efficiency of the field from the sodium plant and the efficiency of the downstream components from the salt-in-tube system to establish the annual delivered energy.

Finally, the reduction in cold salt pumping power was calculated based on the decrease in pumping head for the IFR, and the annual energy delivered was increased by this amount.

The results of scaling the annual reflective and thermal losses are presented in Table 2-2. The PG&E salt-in-tube and sodium systems used different towers and fields, which accounts for the difference in the radiation incident on the

*In the absence of better data, these values were assumed to be uniform over the spectrum (i.e., gray-body values).

Table 2-1. Receiver Performance Parameters

	S-I-T	DAR	IFR (base case)
Absorptance	0.92	0.96	0.92
Emittance	0.89	0.96	0.89
Average temperature	557°C	447°C	534°C
Absorber area	1274 m^2	756 m^2	1022 m^2

receiver. In addition to the average annual field efficiency, the value for radiation incident on the receiver also includes factors to account for losses caused by forced defocusing and plant outages. The combined efficiency of all systems downstream from the receiver (e.g., transport, storage, EPGS) was assumed to be 0.365 (the value for the PG&E salt-in-tube system). Note that the annual energy delivered by the IFR and DAR has been increased by 3,095 MWh to account for the decrease in pumping power caused by the decrease in friction losses. This decrease in pumping power was also calculated with an algorithm developed by Bechtel National Inc. for the PG&E team [3].

The cost of the IFR system was based on the reported costs for the PG&E salt-in-tube receiver system [2]. A detailed cost breakdown for the receiver subsystem was obtained from Bechtel [3], and the cost of the IFR relative to the salt-in-tube receiver was determined on a component-by-component basis. Breakdowns of the receiver component and subsystem costs for the IFR, DAR, and PG&E salt-in-tube receivers are given in Appendix B.

Table 2-2. System Performance Comparison of Annual Energy Values (MWh/year)

	S-I-T	DAR	IFR (base case)
Total radiation incidence on receiver	1,177,379	1,143,614	1,143,614
Reflected losses	94,190	46,431	91,489
Emitted losses	144,818	51,629	103,640
Convective and conductive losses	48,272	22,770	37,071
Total receiver losses	287,280	120,830	232,200
Total energy delivered by the receiver	890,098	1,022,784	911,414
Reduced pumping power		3,095	3,095
Electric energy delivered	325,378	373,663	336,126

Table 2-3 shows the collection of the various component and subsystem costs into the overall plant costs. Other than the receiver, the differences between the cost for the salt-in-tube receiver system and those for the IFR and DAR systems are mostly attributable to the differences in the layout of the heliostat fields for the PG&E design for the salt-in-tube system versus the sodium system.

The parameters used in calculating the LEC values are shown in Table 2-4. The fixed charge rate used in this calculation was 0.105, the value used for the *Utility Study* calculations. As mentioned earlier, the operations and maintenance costs are held uniform for all three systems. The capital cost values are from Table 2-3, and the annual energy values are from Table 2-2.

The predicted LEC for the base-case IFR is lower by approximately 5.7 mils/kWh than the value for the salt-in-tube receiver system. This amount represents about a 5% decrease in the LEC for the salt-in-tube receiver system. About 2% of this decrease is attributable to the decrease in capital cost. The remaining 3% is the result of the improved performance, which is caused primarily by the decrease in receiver size that is made possible by the increased flux limits.

Table 2-3. Plant Capital Cost (in thousands of dollars)

	S-I-T	DAR	IFR	Notes
Direct Costs				
0. Land	1,140	1,045	1,045	
1. Structures & improvement	3,161	3,056	3,056	Smaller land area
2. Collector system	92,241	93,810	93,810	Na system had more heliostats[1]
3. Receiver system	33,205	25,713	26,471	Na tower, salt mechanical parts (except for smaller pumps)
4. Thermal storage system	21,878	21,878	21,878	
5. Steam generation system	14,951	14,951	14,951	
6. Elec. power gen. system	53,587	53,587	53,587	
7. Master control system	1,950	1,950	1,950	
Total Direct Costs	222,113	215,990	216,748	
Indirect costs (22.5%)	49,976	48,598	48,768	
AFDUC (12.15%)	26,991	26,247	26,339	
Total capital cost	299,080	290,835	291,856	
Difference in costs		8,245	7,224	

[1]The heliostat field for the PG&E sodium system had a higher density than the salt system.

Table 2-4. Levelized Energy Cost Analysis[1]

	S-I-T	DAR	IFR
Capital cost (thousands of dollars)	$299,080	$290,835	$291,856
Annual O&M cost (thousands of dollars)	$4,500	$4,500	$4,500
Annual electricity generated (MWh)	325,378	376,760	336,138
LEC ($/kWh)	$0.1103	$0.0930	$0.1046
Percentage difference (based on S-I-T system)		15.72	5.25

[1]Fixed charge rate is 0.105.

The relationship of the LEC figures can be seen graphically in Figure 1-2. The figure also shows that the decrease in LEC for the IFR is not terribly sensitive to the allowable flux levels, as represented by the average flux. At an average flux of 0.73 MW/m^2, the LEC for the DAR is about 85% of that for the salt-in-tube receiver system. However, at this same average flux, the LEC for the IFR is still about 93% of that for the salt-in-tube receiver system, only about 2% lower than for the base case at 0.53 MW/m^2. This difference between the DAR and IFR is attributable to the fact that the lower surface temperature of the DAR significantly reduces the receiver losses.

At the low flux end of the curve, the IFR absorber becomes just as large as the salt-in-tube absorber. Here, the LEC for the IFR is about 97% of the LEC for the salt-in-tube receiver system. About 1% of this difference is caused by the decrease in pumping parasitics associated with the IFR. The remaining 2% derives from the lower capital cost for the IFR.

3.0 CONCLUSIONS

Based on the estimated 5% improvement in LEC, the IFR does not appear to have as strong a potential for economic advantage as the DAR. The LEC improvements for both the IFR and DAR derive in large part from their increased flux levels and concomittant smaller absorber sizes. The average flux level used here for the base-case IFR is based on a preliminary, probably conservative estimate of the stresses introduced in the absorber plate. A higher value for the allowable flux on the IFR absorber will slightly increase the economic benefit of the IFR. However, because of the lower surface temperatures inherently associated with the DAR, the IFR will probably always have larger receiver losses and is unlikely to achieve the same level of LEC reduction as the DAR.

Although the economic benefits of the IFR are not as large as the DAR, there are still several reasons to consider the concept. Fundamentally, the IFR allows the receiver designer to take advantage of the relatively high convection coefficients between the working fluid film and the absorber plate without either (1) exposing the hot working fluid to the ambient or (2) suffering the friction losses and flux constraints associated with tubes. Because of these largely non-economic benefits, the IFR appears to be a concept that offers a potentially viable backup to the current work on the DAR. In fact, should the current efforts on the DAR uncover undesirable behavior associated with exposing the working fluid to the atmosphere, then much of the activity currently directed at the DAR would translate fairly directly to the IFR.

4.0 REFERENCES

1. Anderson, J. V., W. Short, T. Wendelin, and N. Weaver, Direct Absorption Receiver (DAR) Systems Assessment, SERI/TR-253-3162, Golden, CO: Solar Energy Research Institute, August 1987.

2. Solar Central Receiver Technology Advancement for Electric Utility Applications; Phase 1 Summary Review, 1987, San Ramon, CA: Pacific Gas and Electric.

3. Egan, J., and B. Kelly, Private Communication, Bechtel National Inc., San Francisco.

APPENDIX A

FINAL REPORT ON THE IFR CONFIGURATION STUDY FROM SPECO, INC.

FINAL REPORT

FILM RECEIVER COMPONENT ASSESSMENT AND DESIGN STUDIES

PREPARED FOR:

SOLAR ENERGY RESEARCH INSTITUTE
A Division of Midwest Research Institute
1617 Cole Boulevard
Golden, Colorado 80401

Author:

Tibor Buna

SOLAR POWER ENGINEERING CO.
P.O. BOX 91 , MORRISON, CO 80465

NOTICE

This report was prepared as an account of work sponsored by the Solar Energy Research Institute, a Division of Midwest Research Institute, in support of its contract No. DE-AC02-83-CH10093 with the United States Department of Energy. Neither the Solar Energy Research Institute, the Midwest Research Institute, the United States Government, nor the United States Department of Energy, nor any of their employees, nor any of their contractors, subcontractors, or their employees, makes any warranty, express or implied, or assumes any legal liability or responsibility for the accuracy, completeness or usefulness of any information, apparatus, product or process disclosed, or represents that its use would not infringe privately owned rights.

FOREWORD

This report is submitted by Solar Power Engineering Company (SPECO) to Solar Energy Research Institute (SERI) in accordance with the provisions of contract XK606102-1. This contract was under the direction of John V. Anderson of SERI; Tibor Buna was the SPECO program manager. Other SPECO participants contributing to this work included: Dr. Mark Lajczok, Phil Lukens and Bill Miller.

TABLE OF CONTENTS

		Page
1.0	INTRODUCTION AND SUMMARY	1
2.0	OPTICAL DESIGN	7
3.0	IFR CONFIGURATION	9
4.0	THERMO-FLUID PERFORMANCE	16
	4.1 Analytical Approach	16
	4.2 Temperatures and Flow Parameters	18
	4.3 Receiver Efficiency	20
	4.4 The Cavity Effect	25
5.0	THERMOSTRUCTURAL DESIGN	27
6.0	COMPARATIVE COST ANALYSIS	30
7.0	TECHNICAL ISSUES AND CONCERNS	38
8.0	REFERENCES	39

LIST OF FIGURES

		Page
1-1	The Evolution of Receiver Technology	3
1-2	Effect of Wall Thickness on IFR Efficiency and Peak Stress	4
3-1	IFR Design Schematic	10
3-2	Hanger Support Details	11
3-3	Spring Support in Lower Collection Header	11
3-4	Radial Displacement of Absorber Plate	12
3-5	Self-Locking Support Concept	13
4-1	Vertical Flux Density Distribution	19
4-2	Temperature Profiles - 100 % Load	19
4-3	Temperature Profiles - 110 % Load	21
4-4	Temperature Profiles - 20 % Load	21
4-5	IFR Flow Parameters	22
4-6	Film Thickness vs. Distance Along Flow Path	23
4-7	The "Cavity Effect" in the IFR	25
5-1	Effect of Wall Thickness on Thermal Stresses	28

LIST OF TABLES

		Page
1-1	Comparative Cost Summary	6
4-1	Comparison of Thermal Efficiencies	24
6-1	Results of Comparative Cost Analyses	31
6-2	Cost Summary - IFR	32
6-3	Cost Analysis Work Sheet, Sheet 1 of 5	33
6-4	Cost Analysis Work Sheet, Sheet 2 of 5	34
6-5	Cost Analysis Work Sheet, Sheet 3 of 5	35
6-6	Cost Analysis Work Sheet, Sheet 4 of 5	36
6-7	Cost Analysis Work Sheet, Sheet 5 of 5	37

1.0 INTRODUCTION AND SUMMARY

As a follow-on effort to previous work [1] the objective of this study was to extend the original Direct Absorption Receiver (DAR) concept to an Internal Film Receiver (IFR) configuration with the molten salt film flowing inside an external absorber plate. Additionally, an attempt was made to better define some issues related to film receivers, in particular concerning flux limits and warmup strategies; and to further identify technological issues related to both the DAR and the IFR concepts. Per agreement, the selected receiver rating for the study was 190 MWt in order to facilitate direct comparison with the Saguaro design [2] used as a reference basis in the previous DAR study. The choice of the most appropriate overall system type, i.e. north field/cavity vs. surround field/external, was left to the details of the investigation.

It should be noted, however, that the Saguaro design no longer represents the current state of the art of tubular cavity receivers. In a recent study conducted jointly by PG&E and APS [3] a re-assessment of allowable flux limits for a tubular salt receiver in combination with improved heliostat aiming strategies resulted in an improved design with a 46 percent reduction in absorber area and a 30 percent reduction in receiver cost compared to the previous estimates made for the Saguaro receiver. Additionally, a consensus by these utilities came out in favor of the surround field/external configuration primarily because of practical limitations of tube lengths and overall absorber panel and aperture dimensions - hence thermal ratings - of the north field/cavity systems. These recent developments have been taken into account in the assessment of the relative merits of the film receivers in the present study.

As a class of receivers, the DAR and the IFR have a number of inherent characteristics in common:

- High heat transfer rates without the associated pressure drop (or pumping power) penalty necessary with tubular heat exchangers;
- Gravity flows across the heat exchange surfaces and the feed and discharge systems, resulting in an increased number of required control zones but a greatly simplified controller design, when compared to tubular receivers;
- Planar as opposed to tubular heat exchange surfaces, resulting in a reduction of the ratio of heat transfer to radiation intercept area by a factor of π ;
- The capability to operate at or near ambient pressures;
- Simplicity and reduced weight of support structures;
- Strong coupling between thermo-fluid and thermo-structural behavor resulting in potentially significant effects of small structural deformations on flow stability;
- Because of the above, a more closely controlled warmup and salt flow initiation procedure requirement when compared to tubular receivers.

The inherent differences between the IFR and the DAR include:

- The IFR is expected to have lower thermal efficiency and higher thermal stresses than the DAR because of thermal gradients across the wall;
- The DAR is expected to have virtually no flux limitations when using doped salt as the heat transfer fluid.The minimum size of the IFR is flux limited due to thermal stresses associated with wall temperature gradients.

- The IFR does not require dopant management or salt regeneration subsystems;
- The IFR allows more freedom in geometrical configuration and a broader choice of overall designs (including "pressurized structures" suggested by Dr. L.M. Murphy of SERI) than the DAR;
- The IFR can potentially be used for direct heating of fluids other than salt such as for distillation, evaporation, or desalination processes. The DAR would require the use of molten salt or other low vapor pressure liquid as an intermediary heat transfer fluid for such applications.

Consistent with the current evolutionary trend in receiver technology outlined above, a surround field/external type of system with a conical receiver was selected for evaluation. The cone represents the simplest modification of the traditional cylindrical external receiver geometry that provides positive slopes for the internal salt film flow during both "cold" and thermally deformed "hot" operating conditions of the heat transfer surface. (The thermal deformation of a cylinder due to temperature gradients along the flow path would cause negative slopes whose permissible limits could not be determined within the scope of this study). The cone also retains the favorable thermo-structural characteristics associated with a monocoque cylinder.

Using a one-dimensional aiming strategy with aim points along the axis of the cone, the radial dimensions of the cone were determined so as to intecept the largest heliostat images with an assumed Effective Beam Divergence Angle (EBDA)* of 50 minutes of arc, while the axial dimension was "streached out" sufficiently to comply with an assumed peak flux limit of .85 MW/m^2 -adopted from previous tubular receiver studies. The result is a conical receiver that is image-limited** in the radial direction, and flux-limited*** in the axial direction.

A comparison of geometries and dimensions of the active heat absorption surfaces of the IFR and four other receivers is shown in Figure 1-1. The "equivalent external DAR" has an image-limited (for EBDA = 50 min. of arc) cylindrical geometry, and provides a basis for comparing expected area-dependent losses (emission and convection) of the IFR and DAR. In the case of the IFR these losses are wall thickness-dependent, as indicated by the efficiency plot in Figure 1-2, calculated based on the assumption that the reflection losees of the IFR and DAR are the same (6%).

---

* The EBDA is defined as the effective angular size of the reflected sun as "viewed" from the receiver. It incorporates the combined effects of all heliostat beam errors.

** The dimensions of an image-limited receiver are the minimum required to intercept the reflected radiation without constraints imposed by peak flux -or other- limitations.

*** The dimensions of a flux-limited receiver are the minimum required to provide acceptable flux levels and distributions with optimized aiming strategies.

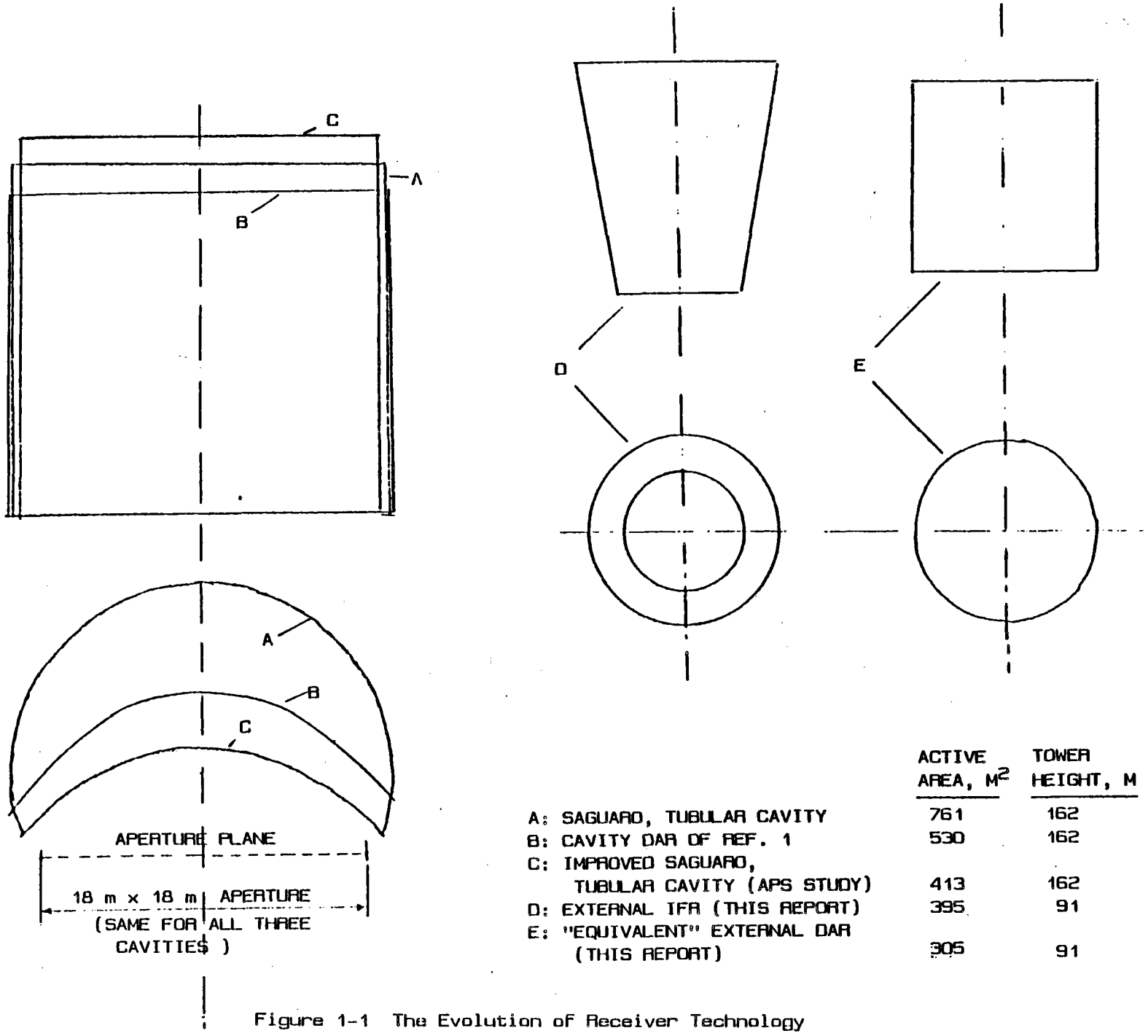

	ACTIVE AREA, M^2	TOWER HEIGHT, M
A: SAGUARO, TUBULAR CAVITY	761	162
B: CAVITY DAR OF REF. 1	530	162
C: IMPROVED SAGUARO, TUBULAR CAVITY (APS STUDY)	413	162
D: EXTERNAL IFR (THIS REPORT)	395	91
E: "EQUIVALENT" EXTERNAL DAR (THIS REPORT)	305	91

Figure 1-1 The Evolution of Receiver Technology

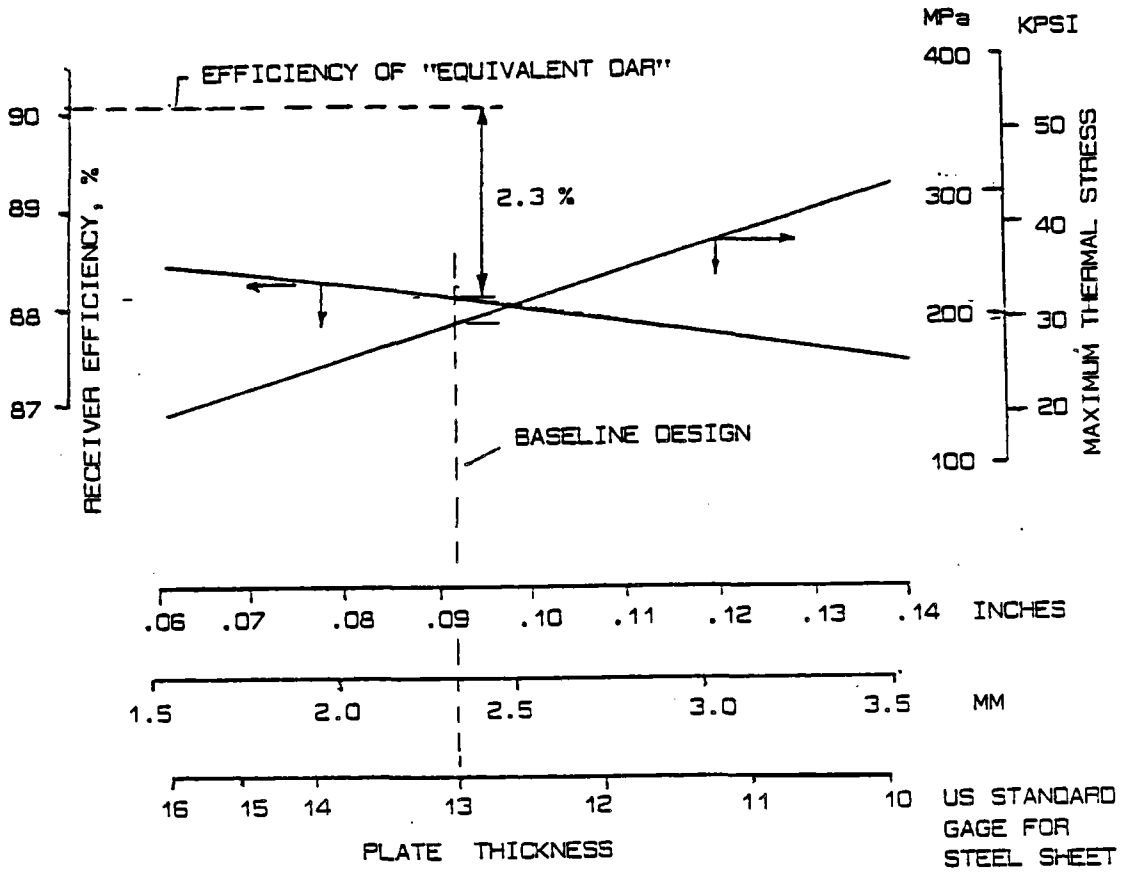

Figure 1-2 Effect of Wall Thickness on IFR Efficiency and Peak Stress

The other key wall thickness-dependent parameter of concern: the maximum thermal stress as is also shown on the figure. For wall thicknesses up to 3.2 mm (1/8 inch) peak stresses compare favorably with current allowables for tubular receivers.

Compariative cost estimates for the IFR and three cavity receivers are shown on Table 1-1. It is readily apparent that the very favorable cost picture indicated on the IFR column of the table is primarily due to the shorter tower and lighter structure associated with the surround field configuration, to which both the IFR and the DAR are readily adaptable.

It is concluded that the IFR concept represents a viable low-cost alternative to both tubular and DAR receivers. At this stage of their development, cost/performance projections for the two film receiver concepts are very similar; however, these projections could change significantly in the near future pending results of ongoing research on doped salt properties and film/air interface transport. The performance -and indeed survival- of both receiver concepts will depend strongly on the development of adequate warmup and salt flow initiation procedures, which should, therefore, be included in the agenda of current research. Within the framework of current commitment to the development of the DAR, the IFR should at least be considered as a backup system to the DAR. The IFR should also be considered as a prime candidate for low pressure process heat applications, such as desalination.

Table 1-1 Comparative Cost Summary

	REFERENCE SAGUARO CAVITY (Reference 2)	APS - IMPROVED CAVITY (Reference 3)	NORTH FIELD CAVITY DAR (Reference 2)	SURROUND FIELD EXTERNAL IFR (This Study)
Basic Receiver Subsystems	10,310,500	7,051,400	2,925,000	1,910,300
Proposed Optional Equipment (Door, Emergency Curtain, Recirculation SS)	553,300	553,300	529,900	
Salt Recirculation & Drain System	3,556,200	3,556,200	2,338,000	1,570,910
Auxiliary & Support Subsystems	491,600	491,600	491,600	491,600
Subtotal Receiver	14,911,600	11,652,500	6,284,500	3,972,800
Tower	5,400,000	5,400,000	4,000,000*	1,500,000*
Total Receiver & Tower	20,311,600	17,052,500	10,284,500	5,472,800

* DAR and IFR tower costs based correlation for Sodium Receivers in Reference 4. Other tower data from salt receiver correlation of same source.

2.0 OPTICAL DESIGN

The first step in the IFR design consisted in defining the geometry and dimensions of the collector field-tower-receiver complex, in conjunction with an appropriate heliostat aiming strategy. In the previous DAR study [1] this process could be accomplished by scaling from the Saguaro design, with some modifications applied to receiver geometry and aiming strategy in order to accommodate the higher flux allowables of the DAR. In the present case this technique could not be used because of inherent dissimilarities in north field and surround field optical configurations. The approach taken was to first establish some rough sizing parameters using the rationale described below, and then applying refinements using the CAD-type DOMAIN PC code, which was modified to accommodate the conical receiver/surround field configuration. The final output of DOMAIN consisted of flux maps and associated aiming strategies that are consistent with the thermal rating, and the thermo-fluid and thermo-structural constraints of the receiver. This approach is an iterative process with thermo-fluid and structural analyses conducted interactively.

The rough sizing of the IFR mentioned above was accomplished by the use of the following rationale applicable to image-limited systems of equal rating. The 190 MWt Saguaro cavity receiver may be "transformed" into an image-limited north field external receiver by replacing its aperture with a heat absorption surface of the same area. Let this area be L^2. It may be assumed that the energy delivered by the collector field is roughly proportional to its area, hence a 190 MWt circular surround field would have approximately the same radius as the Saguaro collector field. A tower half the height of that of the Saguaro plant placed in the center of the surround field will preserve the slant angles of the reflected beams from the farthermost heliostats in the two cases, with the maximum slant range and heliostat image size in the surround field case being only half those of the north field case. Assuming an axi-symmetric radiation field, the image-limited heat absorption surface of the 190 MWt surround field external receiver will be a cylinder with diameter=height=$L/2$, and area $(\pi/4)*L^2$ -or approximately 78.5 percent of that of image-limited external north field receiver.

Since most absorber surfaces become specular reflectors at radiation incident angles greater than about 60 degrees, the diameter of this minimum area receiver must be increased to reduce reflection losses. A factor of $1/\sin(60^0)$ was adopted in this study resulting in an increase in diameter of 15 percent. At higher latitudes another increase in absorber area is required to account for biasing the surround field towards North (or South) in order to compensate for the lower heliostat efficiencies in the southern (or northern) portions of the field. Thus practical considerations lead to a minimum surround field receiver area that is approximately equal to, or slightly larger than, the aperture of an equivalent north field cavity. Since the present analysis is comparative, this second effect due to biassing was neglected in the study for the

sake of simplicity. These considerations apply to the active heat absorption portions of the panels only. Additional panel area must be provided to accommodate boundary layer development in the vicinity of the feed system, and for discharge into the lower manifold.

The cylindrical surface just derived represents an image-limited receiver since no consideration was given to thermo-fluid and/or thermo-structural constraints in the derivation. The .85 MW/m^2 peak flux limit adopted for this study could not be met with this geometry. However, it could potentially be used as the absorber surface for a DAR, which is expected to have virtually no flux limitations. Accordingly, we have labelled this surface "Equivalent External DAR" (Figure 1-1) and used it for comparative purposes. The dimensions of the IFR were derived from this cylinder by increasing its length (to reduce fluxes) and "re-shaping" it into a cone, using the iterative process referred to previously. A five point aiming strategy was used to "flatten out" the flux profile along the flow path. The aim points are located on the vertical axis of the receiver, with the heliostats closer to the tower and having narrower images aimed at the lower portion of the cone.

The active area of the IFR is about 30 percent larger than that of the "Equivalent DAR". As indicated in the subsequent sections, this size allows for significant margins in the design both with regard to stress levels and concerning the 600 C corrosion limit. Accordingly, more detailed design/analyses could indicate potential reductions in the IFR absorber area. As implied above, the IFR collector field is circular with the tower at the center, and it is approximately the same size as that of the Saguaro plant.

The optical design was based on an effective beam divergence angle (EBDA) of 50 minutes of arc, which is considered representative of commercial collector field applications. Since the heliostat images are proportional to the EBDA, the image-limited receiver areas could be further reduced by improvements in heliostat beam quality. For example, since the image-limited area requirements are proportional to the square of the EBDA, the theoretical lower limit for the "Equivalent DAR" using the sun's intercept angle of 32 minutes of arc as the EBDA is 125 m^2 (6.75 m diameter x 5.90 m high).

3.0 IFR CONFIGURATION

The schematic of the IFR design for a 190 MWt nominal rating is shown in Figure 3-1. Major subsystems include: a conical heat absorption surface made of 13 GA (.0919 in, 2.33 mm) 316 SS sheet, main support structure consisting of an 11.2 m diameter upper platform supported by a 3.6 m dia. x 18.3 m high x 12.7 mm (1/2 in) wall CS column, a 3.7 m dia. x 2.0 m high CS cold surge tank, flow controllers, upper manifold and flow feeders, lower header or collection manifold, heat absorption plate supports, a self-locking wind load support structure, insulation and weather protection covers, and an instrumentation and control system.

The conical heat absorption plate is coated on the outside with Pyromark (or equivalent) high-temperature black paint. The radiant energy incident on the outer surface of the cone is absorbed by a flowing molten nitrate salt film on the inside surface of the cone. The heat absorption plate is suspended from the upper support platform by hanger type supports that permit radial thermal expansion but constrain the top of the cone axially and from rotation or tilting in any direction. Details of the hanger type supports are shown in Figure 3-2. The lower rim of the cone is supported in in-plane tension by spring supports mounted integrally within the lower collection header, as shown in Figure 3-3. The header itself is anchored to the lower support plates of the central support column by adjustable anchor rods. This arrangement pre-stresses the heat absorption plate in tension in the cold condition, while allowing for differential expansion -with local variations- between the plate and the header in the hot condition. The anchor rods are mounted in a triangular fashion, similar to the hanger supports, so that they allow radial expansion, but constrain the lower header from motion in other directions.

The conical shape of the heat absorption surface provides a positive slope for the salt film during all operating conditions. The radial displacement of the wall due to thermal expansion varies along the vertical as indicated by the results of a parametric study shown in Figure 3-4. The plate temperature increases, while the cone radius decreases in the downward direction resulting in the slight bulging of the cone in its mid-section.

In order to prevent inward buckling of the heat absorption plate due to wind loads, the support concept shown in Figure 3-5 was devised. The requirement is to allow for free expansion in the outward radial and downward axial directions, while constraining movement of the plate in the inward radial direction. One promising approach to solve this problem would be to pressurize the cone with a slight pressure in the order of 0.2 psi, as suggested by SERI. An evaluation of this approach was outside the scope of the study, hence the mechanical alternative shown in Figure 3-5 is introduced.

The radial force (actually a force of reaction to wind loads) provided by the supports is transmitted to the plate through standoffs (Figure 3-5) which are "cooled" by the flowing salt film during operation. This approach is necessary in order to provide a thermally controlled contact interface between plate and support. During warmup from ambient

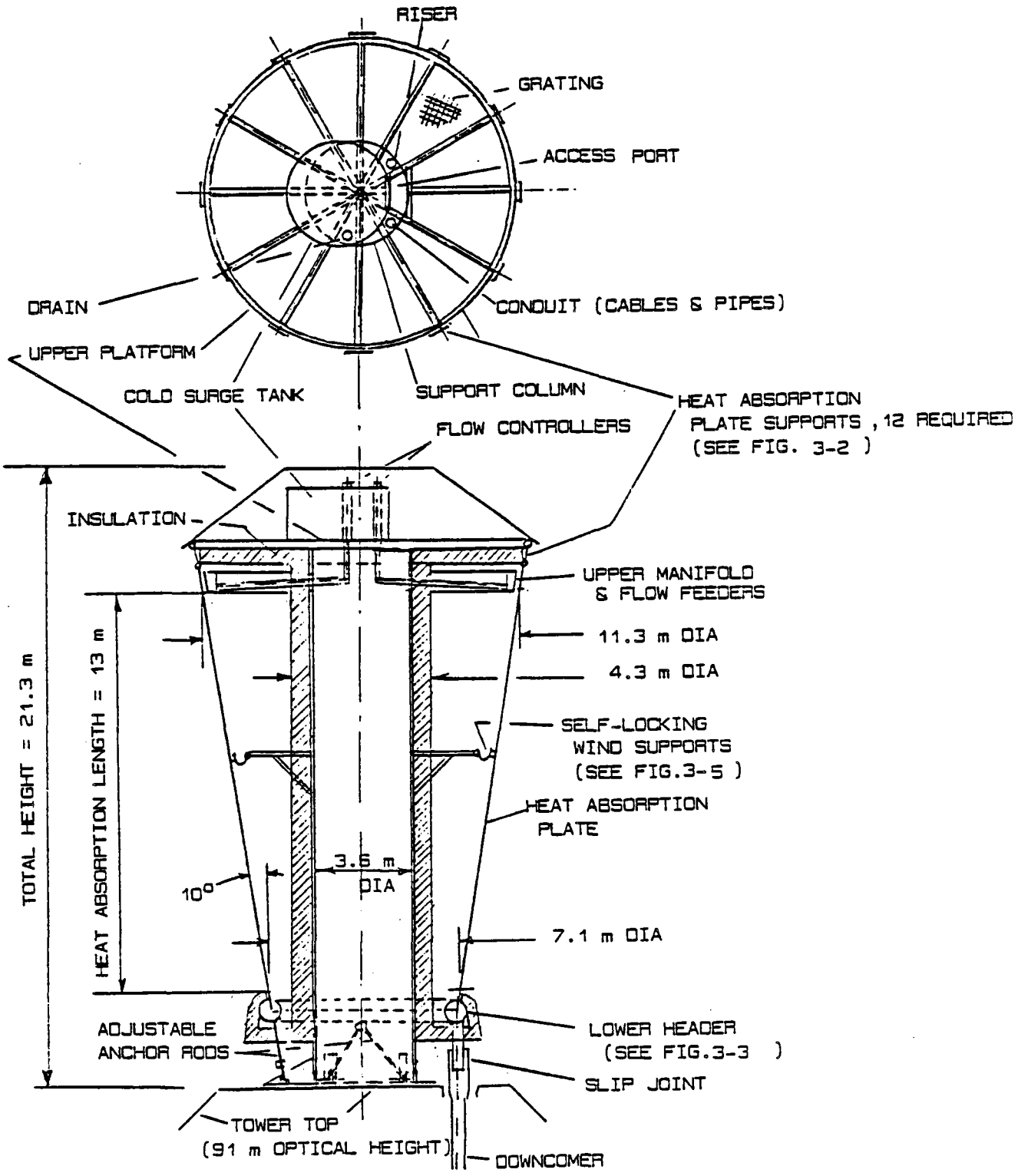

Figure 3-1 IFR Design Schematic

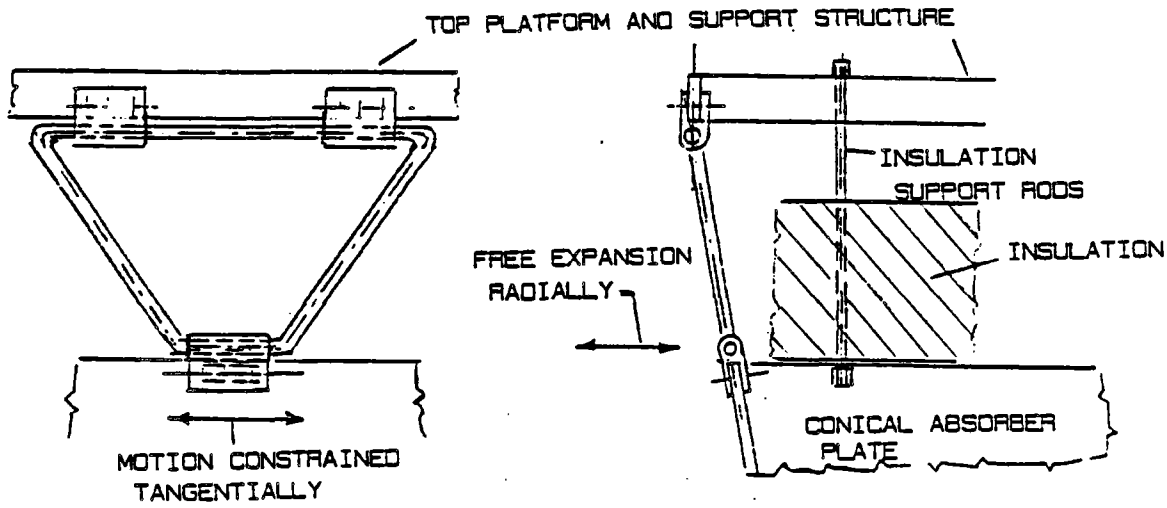

Figure 3-2 Hanger Support Details

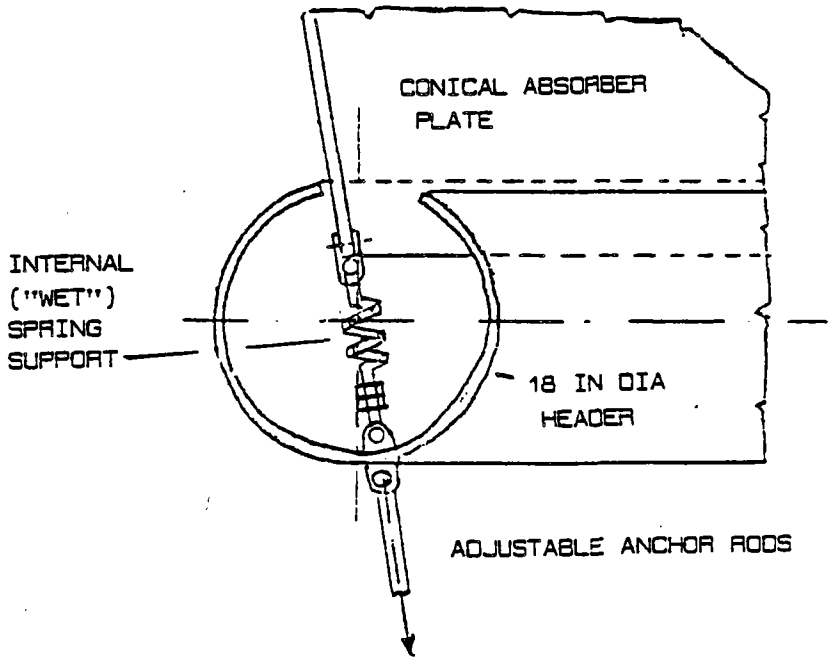

Figure 3-3 Spring Support in Lower Collection Header

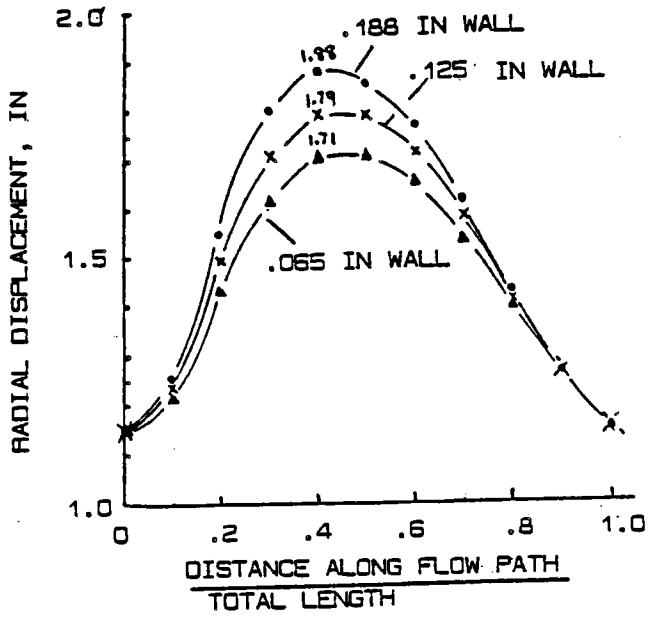

Figure 3-4 Radial Displacement of Absorber Plate

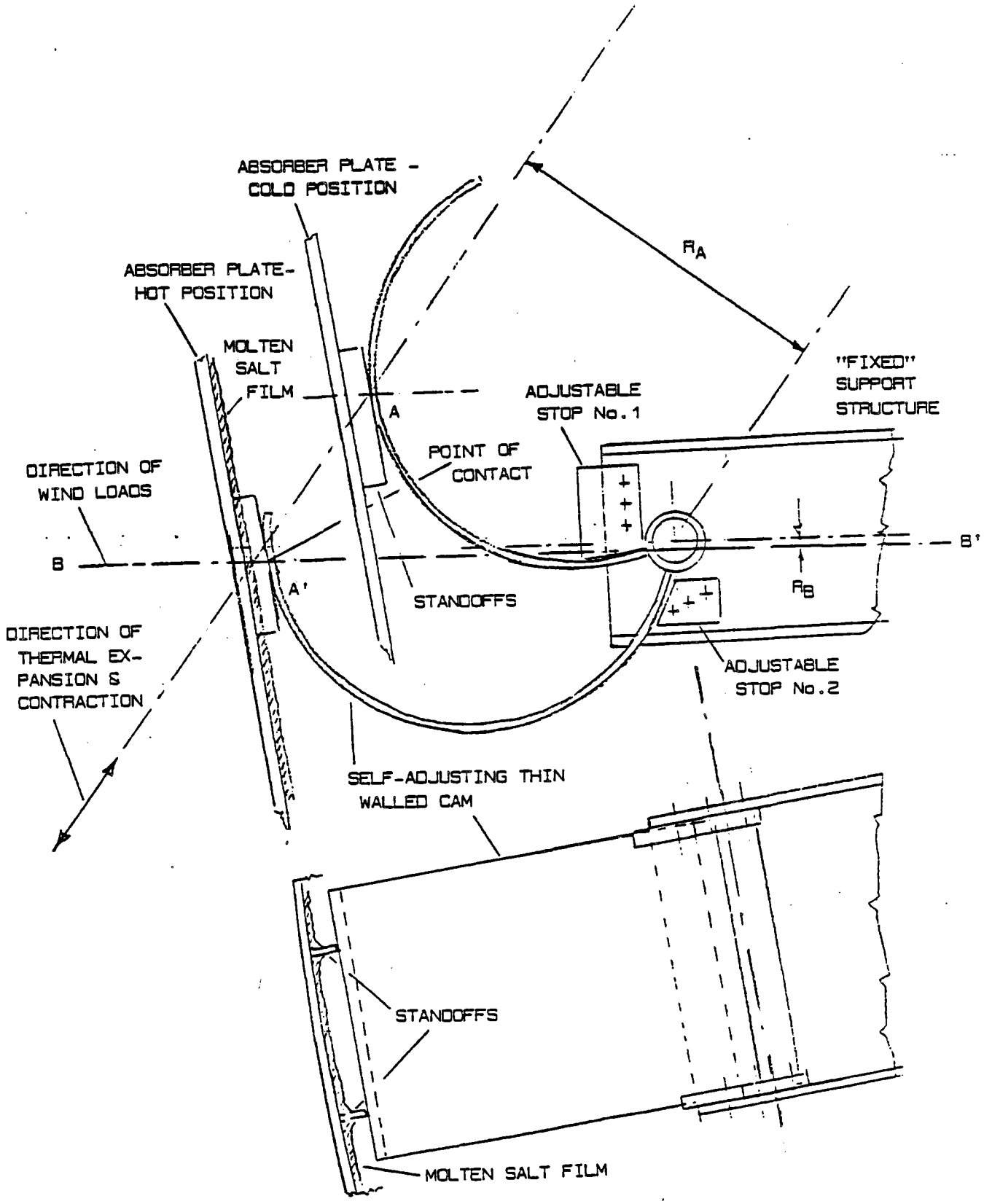

Figure 3-5 Self-Locking Support Concept

to steady state operation, a point A on the standoff will move along a displacement path AA'. The "self-adjusting thin-walled cam" of a semi-circular cross section provides mechanical contact between the standoff and a fixed support structure (e.g. a beam attached to the central support column of the receiver) throughout this motion. In the cold position of the plate inward buckling is prevented by the "adjustable stop No. 1" which constrains the clock-wise rotation of the cam. In the hot position, the wind load acts along line BB' which goes through or closely under the hinge point of the cam. Since the moment arm RB is very small, the cam is in a self-locking position in this case, and the wind forces are transmitted directly to the fixed support structure. The function of the second stop labelled "adjustable stop No. 2" on the figure is only to prevent excessive counter-clockwise rotation of the cam due to gravity in case of loose contact between the cam and the standoffs in this position.

When the plate is cooled from operating to ambient condition, the contact point will start moving in a direction parallel to the line AA' imparting a positive (clock-wise) moment on the cam proportional to the moment arm RA, thus unlocking the cam from its hot self-locking position. The basic idea behind this concept hinges on the fact that local displacements due to wind on one hand, and thermal expansion and contraction on the other, have lines of action at different directions.

The cold surge tank is sized to provide emergency salt flow for approximately 60 seconds (59,000 lbs of salt) to protect the receiver from overheating during a power failure that would result in a loss of power to the heliostats and the salt pumps.

A number of components/subsystems of the IFR are the same or similar to those of the OAR previously reported [1] and are not discussed in detail. They include: the flow controllers, feed manifold and distribution system, instrumentation and control system, and the "slip joint" type of coupling to the downcomer. No recirculation system is included in the present design of the IFR, hence the lower surge tank has also been eliminated in this design. This is consistent with the intent to make this design as simple as possible. The straight downcomer and riser concept previously introduced [1] has been adopted for the IFR.

IFR-specific components requiring development include the self-locking wind supports, the hanger-type heat absorption plate supports, and the support scheme proposed for the lower cone rim and collection header. The other film receiver-specific components are common with the OAR.

In the absence of a recirculation system the operation of the IFR is simpler than that of the previously proposed OAR. Cold salt (288 C, 550 F) is pumped up to the tower and then to an "in-tank" type flow controller [1] in the top surge tank which controls the level in the tank. The cold pump at the bottom of the tower is a single-stage cantilever pump with no bearings or seals in the salt. The salt is fed to the upper manifold and flow feeders through a series of in-tank type controllers which regulate the flow rates through 12 control zones based on temperature measurements at the discharge end of the absorber plate. The hot salt

(566 C, 1050 F) is collected and discharged into the downcomer by the lower header. The plane of the lower header has a 2-percent slope towards the outlet to facilitate the draining process. The slope is set and maintained via the adjustable anchor rods.

In order to avoid thermal shock or permanent thermal deformation in the plate that could lead to local overheating and destruction of the absorber, accurately controlled warmup strategies must be developed for the IFR as well as the DAR. Because the thickness of the salt film is comparable to that of the plate, film receivers are less forgiving to thermal deformations than their tubular counterparts. A case in point: a post mortem report on the 5 MWt MSEE receiver indicated that some of the tubes "looked like spagetti", yet the receiver had performed satisfactorily to the end. It is hard to imagine that a film receiver could survive similar thermal distortions. To maintain the thermo-structural integrity of the plate, a uniform heating of the entire absorber surface is necessary to levels approaching cold salt temperatures. An improperly designed or executed warmup procedure could cause local overheating and destruction of the receiver.

The use of computerized warmup procedures are necessary to accommodate the daily and rapidly changing hourly variations of insolation parameters. Such programs could be incorporated into the central control system software. The energy required to warm up the absorber plate is minimal (on the order of 500 KWH), hence a properly executed warmup should have an insignificant effect on the daily output of the receiver. The central problem lies in the controlled delivery of this energy to the receiver. This is a subject requiring further study.

4.0 THERMO-FLUID PERFORMANCE

4.1 Analytical Approach

Thermo-fluid analyses were conducted with a computer code developed for this application on an IBM System 2 personal computer. With an absorber flux map and absorber geometry as the principal inputs, this program calculates film thickness and velocities, heat transfer coefficients, salt and metal temperatures, and radiation and convection losses from the receiver.

The design/analysis of an external OAR was not within the scope of this program. However, in order to be able to make an assessment of the relative merits of the two film receiver concepts, the radiation and convection losses of the "Equivalent OAR" were also determined by extrapolations from the IFR data. In this procedure it was assumed that the IR and convection losses are proportional to absorber area, that the linear and fourth-power averages of the salt film temperatures of the OAR and IFR are the same, that the surface emissivities and reflection losses of the two receivers are the same, and that the OAR convection losses are increased somewhat by two factors: 1) "induced forced convection" due to the velocity of the flowing film, and 2) the increased "roughness" of the surface due to the rolling waves within the film.

The above assumptions as well as the rest of the inputs to the program reflect the painful absence of directly applicable data at the time of this writing. Most of the literature on falling films were developed for such applications as chemical absorbers, fermenters, condensers, distillation, etc. with strong coupling between heat and mass transfer, and with emphasis on mass transfer. The thermal result sought in such applications is heat transfer <u>through</u> the film rather than <u>into</u> the film as is the case with film receivers. Furthermore, the Reynolds numbers of interest in these applications are generally an order of magnitude lower than those for film receivers. Optical properties of doped salt, as well as empirical data pertaining to transport processes at the salt-metal and salt-air interfaces directly applicable to the scales and conditions representative of solar receivers are yet to be developed.

The analytical model was developed with assumptions and inputs from sources indicated below:

- Wall-to-film heat transfer correlation by Wilke [6] . This is a departure from the approach in the previous study 1 where a correlation by Sandall et al [7] was used. This decision was based on a reexamination of these two papers with the conclusion that Wilke's data more closely represent the conditions with <u>no mass transport</u> across the film/air interface. His correlation shows a much stronger effect of the Reynolds number than that of Sandall, resulting in higher heat transfer coefficients than predicted in the previous study.

- The same thermo-physical properties of nitrate salts as used in the previous study, adopted from [9] .

- An effective solar absorptivity of .94 assumed to be the same for the IFR and the Equivalent DAR. This compares with a measured value of .96 reported in [12], a range of .92 to .96 adopted in [15], and a value of .90 derived for doped salt by Abrams [10] and used in [1]. The assumed 6 percent reflectivity is the largest contributor to losses in the present study, and more accurate values for doped salt could have a significant effect on the relative merits of the DAR.

- Effective receiver emissivity of .9 assumed to be the same for the IFR and DAR.

- Convection losses calculated from combinations of the following elements:

  o Pure natural convection correlation by Siebers et al [14].

  o Forced convection correlation by Siebers et al -Equations 3-3 and 3-5 in [14] -to account for the effect on convective coefficients of the relative salt/air velocity in the DAR.

  o A constant atmospheric forced convection coefficient of 14 W/m - C as suggested by [11].

  o An average mixed coefficient for combined natural and forced convection determined by the method of Siebers et al, also adopted by the DELSOL code [11].

  o An additional correction factor was applied to the DAR convection losses to account for the "roughness" of the film due to surface waves. Following Blass [5] a factor of 1.2 was adopted for this study. This may be conservatively low, since data reported in [8] by Dukler in an earlier paper indicated that a change from weak to well-developed wave structure (due to an increase in Reynolds number) results in an increase in the film/air transport rate of 50 to 75 percent. Furthermore, the well-developed wave structure was obtained at a Reynolds number of only 800, which is two orders of magnitude lower than expected in film receiver applications. The 1.2 "roughness factor" in combination with the other corrections applied to the DAR convection loss has a net effect on receiver efficiency of less than 0.1 percent, primarily because the convection loss itself is small. The net increase in the convection loss is about 7 percent. If the Dukler data is correct, the latter figure changes appreciably.

    It should be noted that the salt/air interface transport processes have dual significance for the DAR: they effect not only the thermal efficiency, but also the absorption of carbon dioxide and water vapor from the air which has a bearing on the design of the salt regeneration system required for the DAR [1].

- The heliostat field was assumed to be circular, with the tower at the center. An essentially uniform circumferential distribution

of incident fluxes was assumed at the "design point" of the receivers. Although this assumption is generally not valid at higher latitudes, it is believed to be acceptable for the purposes of this study. A north-biased field, for example, would have comparable effects on absorber sizes in the case of both the IFR and the Equivalent OAR.

- The allowable fluxes for the IFR were assumed to be the same as for tubular receivers. This assumption is probably conservative since there are no stress concerns associated with front-to-back tube temperature gradients in the IFR. No flux limits apply to the Equivalent OAR.

- Flux distributions and aiming strategies for the IFR were determined by an improved DOMAIN code programmed for the IBM System 2 personal computer. The use of a one-dimensional aiming strategy was adopted as a guideline. As a result, the radial dimensions of the IFR absorber cone are image-limited, with the axial dimensions sized to accommodate an acceptable flux distribution from a thermal stress and corrosion limit standpoint. Two additional considerations should be noted:
  1) The aiming strategy was designed so as to bias the aim points of the heliostats close to the tower (and having narrower images) towards the lower part of the cone.
  2) As indicated in Section 2, the minimum radial dimensions determined from heliostat image considerations in the case of both the IFR and OAR were increased by a factor of $1/\sin(60^0)$ (about 15 percent) in order to minimize specular reflection losses associated with shallow incidence angles.

- The thermo-fluid runs were normalized to an absorbed power of 190 MWt, which was input to the program. The required incident power to account for changing efficiencies in the parametric analyses (as a function of wall thickness, for example) were calculated and checked for their effect on the size of the field and on image sizes. These effects were found to be negligible, however, for the purposes of this analysis.

4.2 Temperatures and Flow Parameters

The vertical flux profiles developed for the IFR by the use of the DOMAIN code are shown in Figure 4-1. The peak fluxes are just under current allowables for tubular receiver [3] and are close to those of the cavity OAR design in [1]. The average incident flux is .53 MW/m^2 or about 20 percent higher than in a tubular cavity of current design. With a single aim point the peak flux would have been 1.36 MW/m^2. The corresponding average incident flux on the Equivalent OAR is .77 MW/m^2.

Figure 4-2 shows the salt and metal temperature profiles for 100 percent power (190 MWt absorbed). The peak temperature of the inner surface of the absorber plate is approximately 28 C below the corrosion limit, which is considered a more than adequate margin. The peak outer wall temperature is also relatively low (622 C, 1150 F).

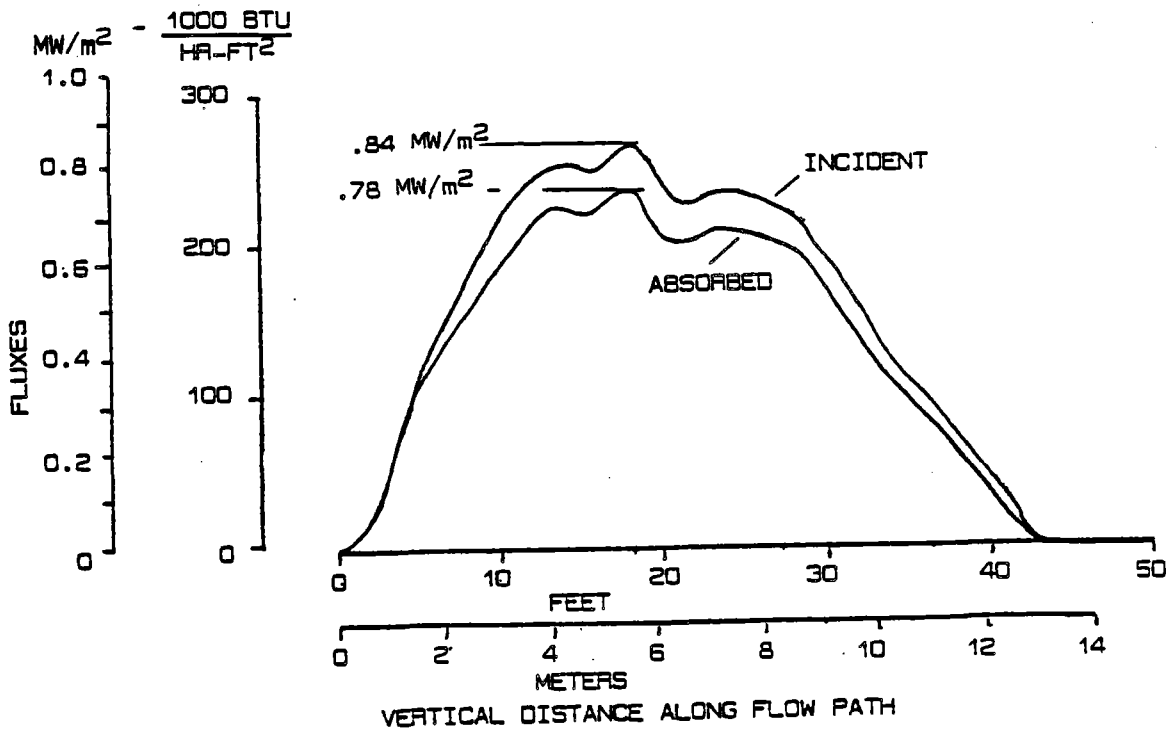

Figure 4-1 Vertical Flux Density Distribution

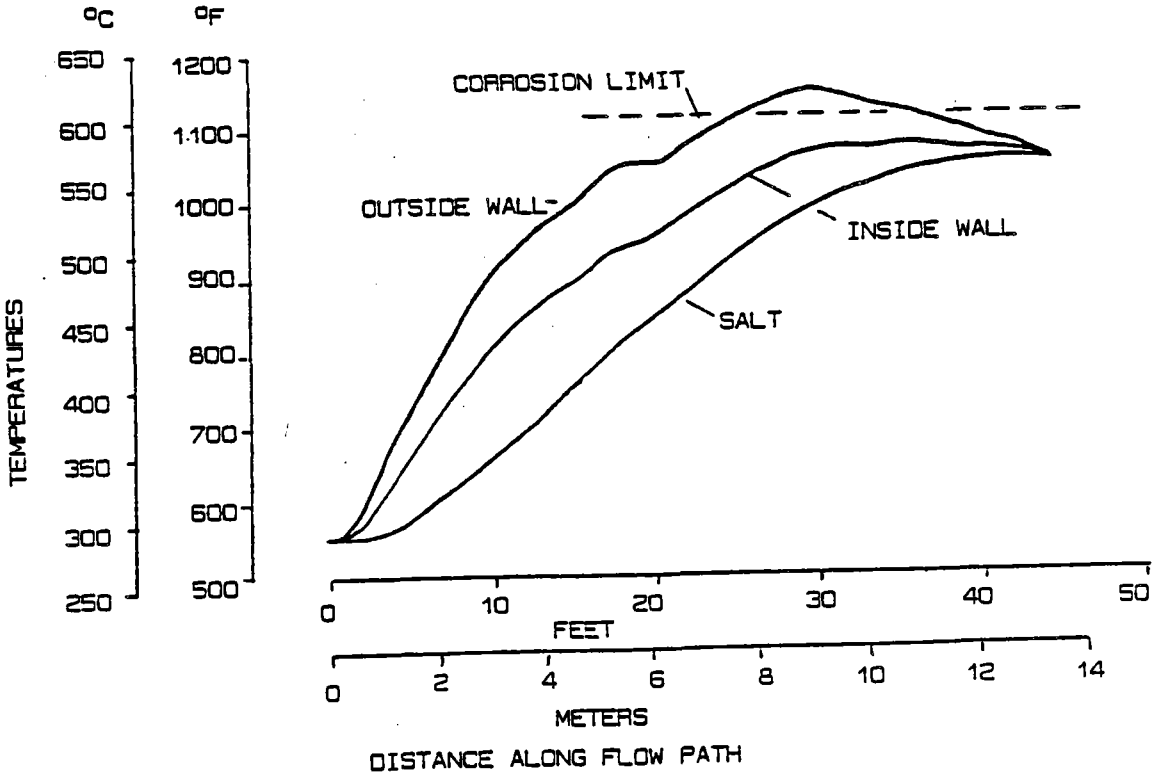

Figure 4-2 Temperature Profiles - 100 % Load

Figures 4-3 and 4-4 show similar profiles for the 110 and 20 percent load cases, respectively. Because of the relatively high heat transfer coefficient at the lower end of the cone, the increase in load to 110 percent has only a minor effect on metal temperatures. At 20 percent load the Reynolds number ranges from 3,000 to 15,000 from the top to the bottom of the cone, and it is well within the high turbulent regime of the film flow. Because of the very small temperature gradients across the wall at low loads, a much higher turndown ratio can be tolerated than indicated here. It should be noted that, unlike in the cavity DAR, the non-linearity of the S-shaped vertical temperature profiles of the absorber plate along the flow path does not contribute significantly to thermal stresses in the IFR because of the axisymmetric configuration of the plate. For the axisymmetric case investigated in this study, the major contributor to thermal stresses is the temperature gradient across the wall, as discussed further in Section 5.

The flow parameters and heat transfer coefficients are shown as a function of distance along the flow path in Figure 4-5. The heat transfer coefficients at the cold salt end of the receiver are comparable to those predicted by the Sandall correlation [7] in the previous report [1]. At the high-temperature end, however, the coefficients according to Wilke [6] are twice as large as those according to Sandall, under otherwise idential conditions.

The film thickness is shown in Figure 4-6. The curve labelled "Wilke" was calculated using Wilke's correlations for the baseline design. The curve labelled "Brotz" is shown for comparison only and was calculated by the use of a correlation developed by Brotz as discussed by Fulford [13]. The Brotz curve was calculated for the same flow rates and temperature conditions as the Wilke curve. Fulford compared various correlations for film thickness and concluded that at high Reynolds numbers the Brotz relationship best fits the available empirical data. Unfortunately, there are no heat transfer data associated with the Brotz correlation. (As far as we can determine from Fulford's review, he studied CO2 absorption). We have included the curve to indicate the uncertainties associated with the use of available data at relatively low Reynolds numbers (such as Wilke and Sandall) to predict performance at high Reynolds numbers.

The effect of the conical shape of the IFR is reflected by the slopes of the velocity and film thickness curves. From top to bottom the velocity increases by 52 percent, while the film thickness increases by 28 percent. These compare with a 10 percent increase in velocity and a 6 percent decrease in film thickness in the cavity DAR of Reference 1.

4.3 Receiver Efficiency

Thermal losses and the efficiency of the IFR as a function of plate thickness is shown in Table 4-1. Comparative data for the Equivalent DAR are also included. As shown, with the assumptions of the analysis, the DAR efficiency exceeds that of the IFR by 2.3 percent. For the same output, this translates into a 2.7 percent increase in heliostat area requirement. Since the collector system cost for a plant of the size under consideration is projected [3] to be about 23 percent, the total

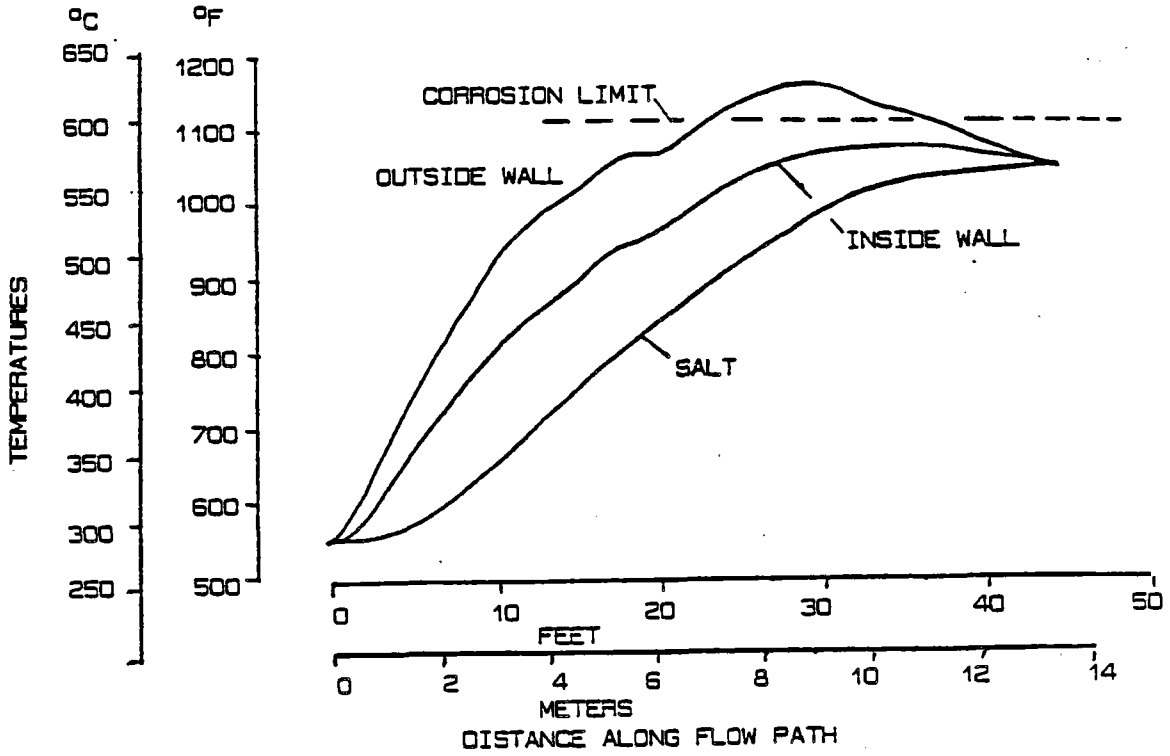

Figure 4-3 Temperature Profiles - 110 % Load

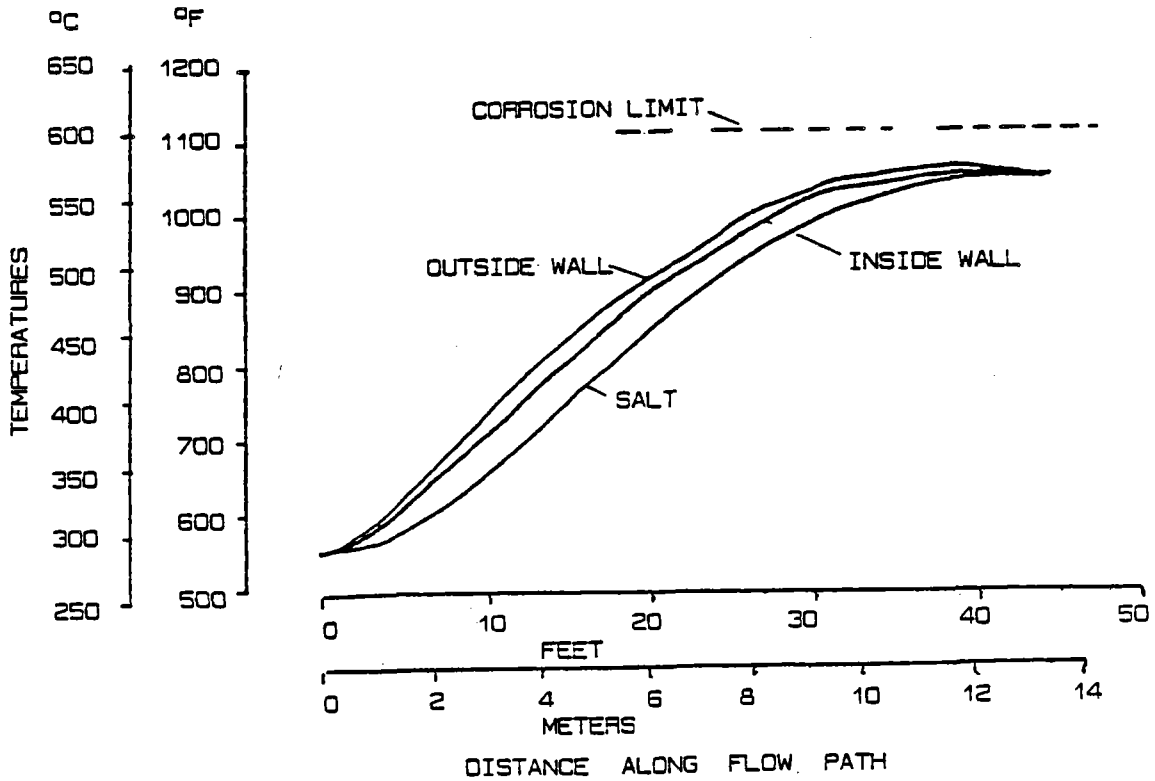

Figure 4-4 Temperature Profiles - 20 % Load

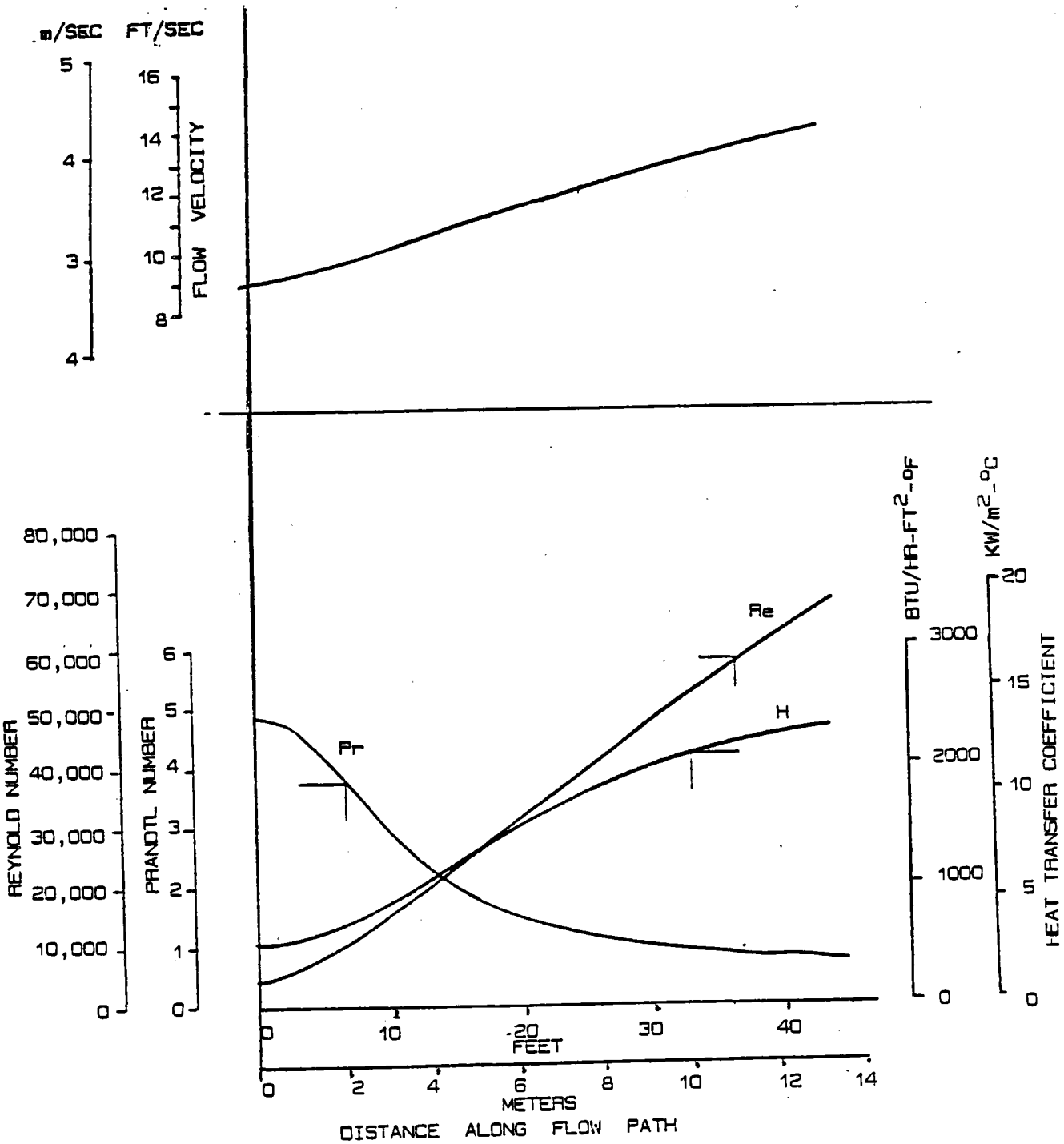

Figure 4-5 IFR Flow Parameters

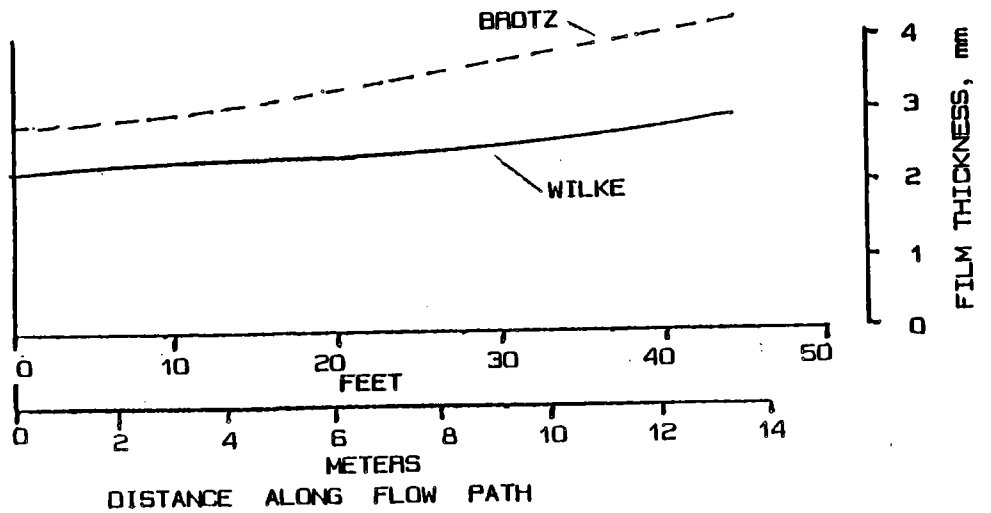

Figure 4-6 Film Thickness vs. Distance Along Flow Path

Table 4-1 Comparison of Thermal Efficiencies

	IFR						
PLATE THICKNESS US STANDARD GAGE INCHES MILLIMETERS	16 .0613 1.56	15 .0689 1.75	14 .0766 1.95	13 .0919 2.33	12 .1072 2.72	11 .1225 3.11	"EQUIVALENT" DAR
RECEIVER LOSSES,%							
CONVECTION	1.4	1.5	1.5	1.5	1.5	1.5	1.2
IR RADIATION	4.1	4.1	4.3	4.4	4.7	4.9	2.4
REFLECTION (ASSUED)	6.0	6.0	6.0	6.0	6.0	6.0	6.0
CONDUCTION (ASSUMED)	0.2	0.2	0.2	0.2	0.2	0.2	0.2
RECEIVER EFFICIENCY,%	88.3	88.2	88.0	87.9	87.6	87.4	90.2
INPUT REQUIRED FOR 190 MWt OUTPUT, MW	215.2	215.4	215.9	216.2	216.9	217.4	210.6
				BASELINE			

effect on plant cost is estimated at 2.3 x 0.23 = 0.53 percent. This estimate is "soft", however, because of the uncertainties in the underlying assumptions of the analysis.

4.4 The Cavity Effect

A unique feature of the IFR is its capability to transfer radiant energy internally among its various active and inactive surfaces and structural support elements. This is expected to minimize thermal gradients during low load operation, warmup, and cloud transients. Another potential use of this capability is for receiver warmup by internal convective and/or radiative heat sources. One method could be the use of recirculating "cold" salt film flowing on a "sacrificial" internal substrate, such as the lagging on the insulation of the central support column, to provide warmup energy to the absorber plate by radiation. Here "sacrificial" implies that such a substrate could be subjected to thermal deformation and buckling due to thermal shock at the initiation of salt flow without detrimental consequences on receiver performance.

A detailed evaluation of the merits of the cavity effect was not within the scope of this study. However, a calculation was performed of representative radiation interchange factors with the result shown in Figure 4-7. The numbers represent black body view factors only, without consideration of additional radiant interchange by reflection and reradiation. Note that the exchange factors for the absorber into itself are about 0.3 to 0.4, while the exchange factors from the absorber to the inner cylinder are 0.2 to 0.5. These data indicate that the problem is worth looking into.

ELEVATION, Z, m	BLACK BODY VIEW FACTOR FROM ELEMENTAL AREA ON ABSORBER PLATE TO:			
	ABSORBER PLATE F_{11}	INNER CYLINDER F_{12}	TOP INSUL. F13	BOTTOM INSUL. & HEADER F14
1.5	.33	.51	.05	.11
3.5	.40	.50	.05	.05
5.5	.42	.47	.07	.07
7.5	.44	.42	.11	.03
9.5	.41	.39	.18	.02
11.5	.35	.30	.34	.01
13.5	.27	.18	.54	.01

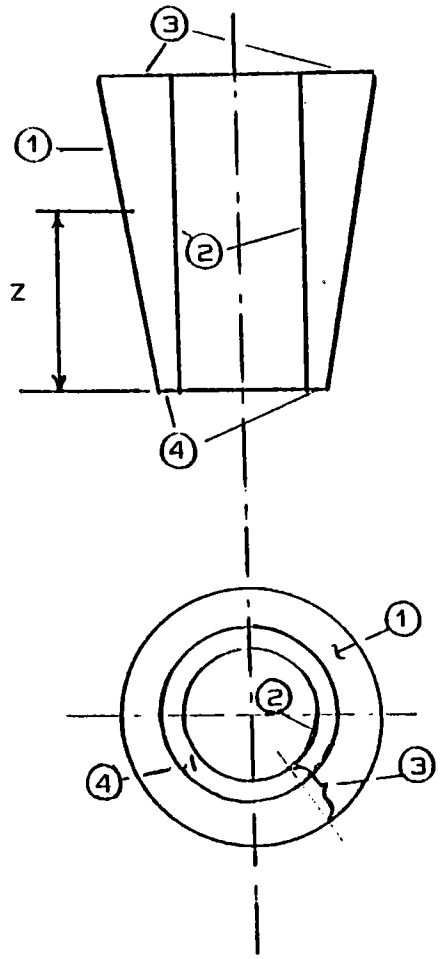

Figure 4-7 The "Cavity Effect" in the IFR

5.0 THERMOSTRUCTURAL DESIGN

The absorber plate support approach was developed as a result of a series of parametric thermostructural analyses conducted with a commercially available finite element PC code. The results have clearly indicated that a fully-constrained plate would develop unacceptable thermal stresses (as expected); that the thermal stresses are minimized if the plate is allowed to expand freely in the radial and axial directions; and that the principal contributors to thermal stresses in the latter case are the temperature gradients across the wall. Due to the limited scope of the study, axisymmetric cases only were evaluated .

Contrary to expectations on the basis of the previous study results [1], the effect of the non-linearity of temperature profiles in the axial direction was shown to be negligible. Since these non-linearities in the cavity DAR and the IFR are quite similar, and since the absorber plates in both cases are supported in quasi-free suspension, the difference in behavor was attributed to the cylindrical geometry of the IFR. Accordingly, some trial runs were made with analytical models of simple flat plates and cylinders subjected to sharp axial thermal gradients, with the result that -for otherwise identical conditions- the stresses in the plates were an order to magnitude larger than those in the cylinders.

A quick review of some of the classical thermostructural literature revealed that Hartog [16] -among others- has shown over forty years ago that the stresses in a flat plate are very much more serious than those in a tube of comparable dimensions and having a comparable axial temperature distribution. This apparent immunity to axial thermal loading in cylinders depends on the value of the dimensionless parameter $L/\sqrt{Rt}$ according to Hartog, where L is the length of the temperature wave (assumed sinusoidal in his analysis), R is the radius of the cylinder, and t is the wall thickness. For values of this parameter larger than about 10, the stresses are negligible. This definitely is the case with the IFR.

Representative thermal stress plots with wall thickness as a parameter are shown in Figure 5-1. The peak stresses are proportional to the wall thickness (approximately) and are located in the vicinity of the 30-percent point in the flow path. As was indicated in Figures 4-2 and 4-3, the peak metal temperatures at that location are of the order of 550 C. Conversely, the highest temperature regions of the plate (about 650 C) correspond to relatively low stresses.

The finite-element code used in these studies predicts the thermal load (eigen values) and mode (wavelength) associated with incipient buckling. It is not capable, however, of analysing post-buckling behavor. In order to obtain some insight into the post-buckling behavor of the plate following severe thermal shock, we have conducted a series of simple experiments with stainless steel foils partially dipped in hot (450 C) molten nitrate salt. The foil thickness was varied from 0.001 to 0.010 inches, and the depth of submersion from 1/10 to 1/2 of the height of the plate. The samples were suspended at one point at their upper edges, and were allowed to expand in any direction freely. The salt and ambient temperatures were measured. In the absence of other

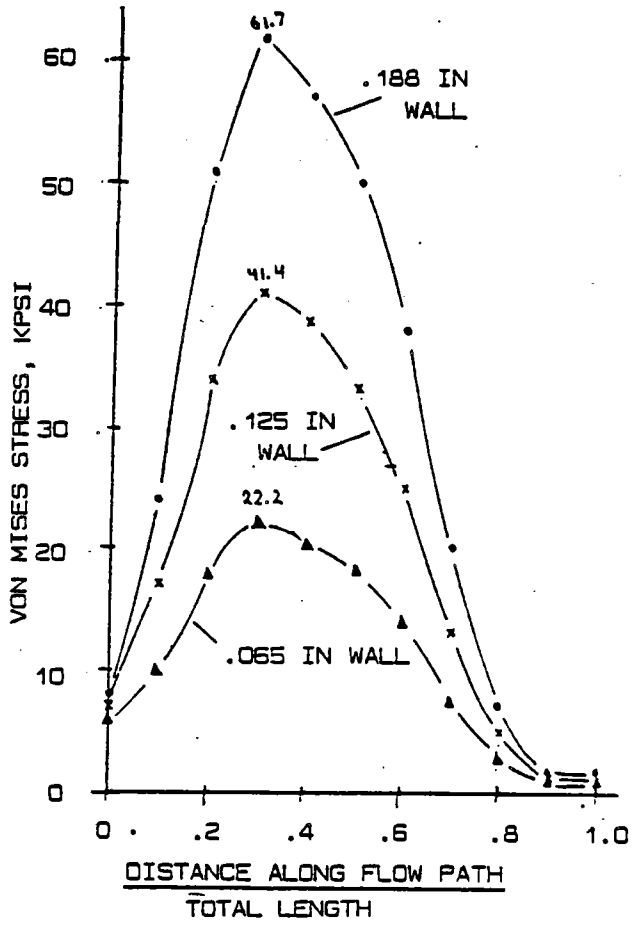

Figure 5-1 Effect of Wall Thickness on Thermal Stresses

instrumentation, the post-buckling deformation of the samples could only be evaluated qualitatively, by visual observation. Additional tests were conducted by pouring a narrow stream of hot salt on foil samples at ambient temperature. These tests were intended to simulate failure modes associated with uneven initiation of salt flow during receiver startup.

The test results indicated that:

- In most cases (but not always) the deformed areas corresponded to the general location of maximum stresses predicted by elastic analyses for the same thermal loading. These areas did not necessarily occur close to the air-liquid interfaces.

- Two basic types of failure modes were observed: 1) a sinusoidal pattern resembling a corrugated plate, usually within the submerged portion of the sample; and 2) a two-dimensional, irregular, criss-cross type of deformation within (predicted) local high-stress areas, usually above the submerged portions of the samples.

- The failure mode associated with the narrow rivulet of hot salt poured on a cold plate was of the first kind, except that the corrugations in this case were horizontal.

- There was no "creeping" of the molten salt due to surface tension observed on either the samples or the walls of the pot in which the salt was melted.

- The wavelengths of the deformed (buckled) samples did not correspond to the predictions of incipient failure modes by the finite difference code. It appears that in order to absorb the strain energy associated with the sudden exposure to the hot salt, the plate (or foil) resorted to higher modes of deformation than predicted for the relatively benign incipient buckling case.

The results of these tests, althogy qualitative, clearly indicate the need for further study in the area of post-buckling behavor, and/or the need for developing safe, accurately controlled, warmup procedures, so that unacceptable permanent local deformations of the absorber plate can be prevented.

Following criteria established for previous projects [2, 3] , the stagnation pressure due to maximum operational wind loads was calculated to be 1 psi. For sizing the structural supports, a cosine distribution of wind pressure acting around the leading semi-circumference of the receiver was assumed.

In view of the conceptual nature of the study, no consideration was given to seismic loads.

6.0 COMPARATIVE COST ANALYSIS

In compliance with the staement of work, a comparative cost analysis of the IFR was performed using the format and cost factors developed by Kaiser Engineers [17] and successfully employed to compare the relative merits of the DAR with the Saguaro design in the previous study [1]. As indicated earlier, the Saguaro receiver is no longer representative of the sate of the art of tubular cavity receivers: a re-assessment of flux allowables in combination with an improved aiming strategy resulted in a greatly improved design and a 30 percent reduction in cost [3]. As indicated below, this development has diminished somewhat - although not decisively - the relative merits of film receivers in general, and of the DAR in particular. Additionally, the current thrust in technology has shifted from north-field/cavity to surround-field/external receivers primarily because of inherent size limitations of the north-field tubular receiver systems considered for utility applications. Accordingly, comparing the IFR with external rather than cavity DAR and tubular receivers should have been the preferred approach, but could not be accomplished within the limited scope of the study.

While preparing the detailed work sheets of the cost analysis it has become increasingly evident that the fluid systems and structural support requirements of the external IFR and DAR should be very similar, and we believe that it can be safely concluded that, when fully developed, there will be no significant difference in cost between the two. Furthermore, a number of components and subsystems are not strongly dependent on the type of system they support, and their cost data could be directly adopted from the previous report [1] . Similarily, the various "fringe benefits" - such as low pumping power and increased reliability - listed in the previous report apply to both receivers and both system types, and have not been re-emphasised in the present cost analysis.

There are two summary sheets included: Tables 6-1 and 6-2. The former compares the costs of the major subsystems of the external IFR developed in the present study with the cavity DAR of [1] , and the "old" and "new" Saguaro designs from [2] and [3] , respectively. We have included tower cost estimates based on a correlation in [4] to indicate the related cost savings associated with the external system: The receiver and tower costs now become comparable. Note that most of the indicated "savings" realized by the IFR when compared to the DAR on this table are due to two factors: 1) the elimination of "optional" subsystems - i.e. subsystems whose cost cannot be decisively justified at the present stage of evolution; and 2) the savings associated with the reduced tower height of external systems. Similar cost savings could be applied to an external DAR.

It is clear from Table 6-1 that, in spite of recent improvements in their tubular counterparts, film receivers still maintain an overwhelming cost advantage.

Table 6-2 is the summary sheet of the detailed cost data developed for the IFR. The work sheets containing the supporting data are included as Tables 6-3 through 6-7.

Table 6-1 Results of Comparative Cost Analyses

	REFERENCE SAGUARO CAVITY DESIGN	APS IMPROVED CAVITY DESIGN	NORTH FIELD CAVITY DAR	SURROUND FIELD EXTERNAL IFR	REMARKS
RECEIVER					
Structure	3,393,700		1,278,200	598,350	IFR/DAR Weight Ratio = 0.4:1
Absorber Panels	4,247,200		839,800	587,288	
Surge Tanks	571,100		164,700	82,350	
Manifold Piping	1,945,900		489,700	489,700	
Monorail	113,900		113,900	113,900	
Fire Protection	21,400		21,400	21,400	
Lightning Protection	17,300		17,300	17,300	
Subtotal Basic SS's	10,310,500	7,051,360	2,925,000	1,910,288	APS vs SAGUARO : 30% Cost Reduction
Cavity Door	553,300	553,300			
Emergency Curtain			98,400		
Recirculation SS			431,500		
Subtotal Optional SS's	553,300	553,300	529,900		
SALT CIRC. & DRAIN SYSTEM					IFR/DAR Tower Height Ratio = 0.56 : 1
Riser / Downcomer	2,617,600		1,702,200	935,110	
Cold Salt Pumps	677,800		422,100	422,100	
Fire Protection	17,300		17,300	17,300	
Electrical	243,500		196,400	196,400	
Subtotal Circ. & Drain	3,556,200	3,556,200	2,338,000	1,570,910	
AUXILIARY SYSTEMS					
Common Instrumentation	49,600		49,600	49,600	
Power & Control Wiring	215,400		215,400	215,400	
Communications	14,200		14,200	14,200	
Lightning Protection	212,400		212,400	212,400	
Subtotal Support SS's	491,600	491,600	491,600	491,600	
TOWER	5,400,000	5,400,000	4,000,000	1,500,000	"Sodium" Cost vs. Height Curve from [4] was used for DAR & IFR
TOTAL RECEIVER & TOWER	20,311,600	17,052,460	10,284,500	5,472,800	

Table 6-2 Cost Summary - IFR

	MANHOURS	LABOR AND BURDEN	EQUIPMENT USAGE	MATERIALS	EQUIPMENT	TOTAL DIRECT	CONTRACTOR OH AND P	SALES TAX (6 %)	TOTAL CONSTRUCTION
RECEIVER									
STRUCTURE	5,534	207,770	27,515	250,801	0	486,086	97,219	15,048	598,353
ABSORBER PANELS	6,056	225,460	18,600	85,650	138,968	468,678	93,694	13,438	575,810
SURGE TANKS	650	24,000	1,400	14,000	110,000	149,400	7,800	7,500	164,700
RECIRCULATION SYSTEM	NOT USED								
MANIFOLD PIPING	6,834	256,400	53,600	83,400	10,000	403,400	80,700	5,600	489,700
MONORAIL	240	9,000	1,700	4,500	90,000	105,200	3,000	5,700	113,900
FIRE PROTECTION	360	14,000	1,700	5,700		21,400			21,400
LIGHTNING PROTECTION	233	8,100	700	5,400		14,200	2,800	300	17,300
SUBTOTAL RECEIVER	19,907	744,730	105,215	449,451	348,968	1,648,364	285,213	47,586	1,981,163
SALT CIRCULATION AND DRAIN SYSTEM									
RISER/DOWNCOMER	7,369	286,880	19,525	430,650		755,425	152,790	26,895	935,110
COLD SALT PUMPS	1,350	50,300	10,000		330,000	390,300	12,000	19,800	422,100
FIRE PROTECTION	35	1,400	200	2,600		4,200	800	200	5,200
ELECTRICAL MOTOR CONTROL,WIRING ELECTR. INSTR	1,410	49,400	4,000	105,000		158,400	31,700	6,300	196,400
SUBTOTAL CIRCULATION AND DRAIN SYSTEM	10,164	387,980	33,725	538,250	330,000	1,308,325	197,290	53,195	1,558,810
COMMON INSTRUMENTATION		20,300	1,600	18,500		40,400	8,100	1,100	49,600
POWER & CONTROL WIRING		101.900	8,200	66,100		176,200	35,200	4,000	215,400
COMMUNICATIONS	92	3,200	300	7,900		11,400	2,300	500	14,200
EMERGENCY CURTAIN	NOT USED								
LIGHTING (TOWER & REC.)	3,180	111,300	8,900	54,100		174,300	34,900	3,200	212,400
TOTAL		1,369,410	157,940	1,134,301	678,968	3,358,989	563,003	109,582	4,031,573

Table 6-3 Cost Analysis Work Sheet
Sheet 1 of 5

	QUANTITY	UNITS MH	UNITS EU	UNITS MAT	MANHOURS	LABOR RATE	LABOR & BURDEN	EQUIPMENT USAGE	MATERIALS	EQUIPMENT	TOTAL DIRECT	CONTRACTOR OH & P	SALES TAX (6%)	TOTAL CONSTRUCTION
RECEIVER STRUCTURE														
STRUCTURAL STEEL														
LIGHT	3 TN	30	200	1,500	90	37.32	3,359	600	4,500	0	8,459	1,692	270	10,421
HEAVY	64 TN	21	150	900	1,344	37.32	50,158	9,600	57,600	0	117,358	23,472	3,456	144,286
MISCELLANEOUS STEEL														
HANDRAIL	440 LF	.3	.25	30	132	37.32	4,926	110	13,200	0	18,236	3,647	792	22,675
GRATING	1,250 SF	.3	.25	12	375	37.32	13,995	313	15,000	0	29,308	5,862	900	36,070
STAIRS	284 LF	1	4	110	284	37.32	10,599	1,136	31,240	0	42,975	8,595	1,874	53,444
LADDERS	45 LF	.3	.25	30	14	37.32	522	12	1,350	0	1,884	377	81	2,342
INSULATION & LAGGING														
INSULATION	3,662 SF	.1	.25	15	366	40.71	14,900	916	54,930	0	70,746	14,149	3,296	88,191
LAGGING	3,662 SF	.3	1.25	7.75	1,099	37.32	41,015	4,578	28,381	0	73,974	14,795	1,703	90,472
ROOFING & FLOORING														
STEEL & STEEL PLATE	3 TN	60	350	1,000	180	37.32	6,718	1,050	3,000	0	10,768	2,154	180	13,102
INSULATION	2,000 SF	.1	.25	15	200	37.32	7,464	500	30,000	0	37,964	7,593	1,800	47,357
TOUCH UP PAINTING - STEEL	290 TN	5	30	40	1,450	37.32	54,114	8,700	11,600	0	74,414	14,883	696	89,993
TOTAL STRUCTURE					5,534		207,770	27,515	250,801		486,086	97,219	15,048	598,353

Table 6-4 Cost Analysis Work Sheet
Sheet 2 of 5

	QUANTITY	UNITS MH	UNITS MAT	MANHOURS	LABOR RATE	LABOR & BURDEN	EQUIPMENT USAGE	MATERIALS	EQUIPMENT	TOTAL DIRECT	CONTRACTOR OH & P	SALES TAX (6%)	TOTAL CONSTRUCTION
ABSORBER PANELS													
FABRICATION													
PANEL	18,400 LB	.04	4.75	740	25	18,500	0	87,780	0	106,280			
PANEL ATTACHMENTS	48 EA	3.0	4.75	144	25	3,600	0	228	0	3,828			
INSULATION	250 SF	.167	10.5	42	25	1,050	0	2,625	0	3,675			
LAGGING, SS	150 SF	.2	3	30	25	750	0	450	0	1,200			
PANEL/STRUCTURAL													
FRAMING	875 LB	.04	4.75	35	25	875	0	4,200	0	5,075			
HANGERS	12 EA	5	150	60	25	1,500	0	1,800	0	3,300			
SUPPORT STANDOFFS	24 EA	3	5	72	25	1,800	0	120	0	1,920			
COLLECTOR HEADER	1,500 LB	.04	4.75	60	25	400	0	2,400	0	2,800			
SUBTOTAL FABRICATION				1,183		28,475		99,603		128,078			
FACTORY INDIRECTS						20,000				20,000			
COST PER PANEL										148,078			
FURNISH AND INSTALL	1 EA	4,000		4,000	37.32	149,300	15,000	0	148,078	312,378	62,475	8,885	383,738
INSULATION	3,700 SF	.167	10.5	620	37.32	23,060	0	38,850	0	61,910	12,400	2,330	76,640
LAGGING	3,700 SF	.20	3	740	37.32	27,600	0	11,100	0	38,700	7,740	670	47,110
PANEL INSTRUMENTS				300	38.70	11,600	2,500	30,000	0	44,100	8,800	1,800	54,700
ELECTR. INSTR.				396	35.00	13,900	1,100	5,700	0	20,700	4,100	300	25,100
TOTAL PANELS				6,065		225,460	18,600	85,650	148,078	477,788	95,515	13,985	587,288

Table 6-5 Cost Analysis Work Sheet
Sheet 3 of 5

	QUANTITY / UNITS				MANHOURS	LABOR RATE	LABOR AND BURDEN	EQUIPMENT USAGE	MATERIALS	EQUIPMENT	TOTAL DIRECT	CONTRACTOR OH & P	SALES TAX	TOTAL CONSTRUCTION
	MH	EU	E											
RISER / DOWNCOMER														
PIPING AND VALVES AVG. DIA. 15"	600 LF				5,180	38.78	200,950	11,000	241,340		454,960	91,025	14,465	560,450
PIPE INSULATION	600 LF				1,694	40.25	68,000	7,700	134,365		226,765	45,375	9,075	281,215
INLINE INSTRU-MENTATION	1 LS				165	38.78	6,380	550	52,195		59,125	13,475	3,025	75,625
HEAT TRACING	1 LS				330	35.00	11,550	275	2,750		14,575	2,915	330	17,820
			SUBTOTAL		7,369		286,880	19,525	430,650		755,725	152,790	26,895	935,110
COLD SALT PUMPS 2050 GPM 700 ' IDH 1000 HP EL.DRIVE	3 EA	450	5000	110,000	1,350	37.32	50,300	10,000		330,000	390,300	12,000	19,800	422,100

Table 6-6 Cost Analysis Work Sheet
Sheet 4 of 5

	QUANTITY/UNITS				MANHOURS	LABOR RATE	LABOR & BURDEN	EQUIPMENT USAGE	MATERIAL	EQUIPMENT	TOTAL DIRECT	CONTRACTOR OH & P	SALES TAX 6%	TOTAL CONSTRUCTION
		HH	EU	E										
SURGE TANKS														
INLET TANK SS 5000 LBS, 12'DIA x 6' x 0.25" WALL	1 EA	100	500	55,000	100	37.32	3,700	500		55,000	59,200	800	3,300	63,300
OUTLET TANK SS 5000 LBS 12' DIA x 6' x 0.25" WALL	1 EA	100	500	55,000	100	37.32	3,700	500		55,000	59,200	800	3,300	63,300
INSTRUMENTATION						- WITH MANIFOLD PIPING -								
TANK INSULATION	900 SF	0.167	10.5		150	37.32	5,600	100	9,500		15,200	3,000	600	18,800
LAGGING	1,000 SF	0.20	3.0		200	37.32	7,500		3,000		10,500	2,100	200	12,800
HEAT TRACING	1,000 LF	0.10	1.5		100	35.00	3,500	300	1,500		5,300	1,100	100	6,500
SUBTOTAL SURGE TANKS					650		24,000	1,400	14,000	110,000	149,400	7,800	7,500	164,700
MANIFOLD PIPING														
PIPING AND MATERIAL	7,750 LB	0.80	6.25		4,000	38.78	155,100	50,000	48,500		253,600	50,700	2,900	307,200
FLOW CONTROLS	10 EA	40		10,000	400	38.78	15,600			10,000	25,600	5,100	600	31,300

Table 6-7 Cost Analysis Work Sheet
Sheet 5 of 5

	QUANTITY/UNITS	MH	EU	MAT	E	MANHOURS	LABOR RATE	LABOR & BURDEN	EQUIPMENT USAGE	MATERIAL	EQUIPMENT	TOTAL DIRECT	CONTRACTOR OH & P	SALES TAX 6%	TOTAL CONSTRUCTION
INSULATION	600 SF	0.167	6.25			100	37.32	3,700		6,300		10,000	2,000	400	12,400
LAGGING	650 SF	0.20	10.5			130	37.32	4,900		2,000		6,900	1,400	100	8,400
ELECTRICAL INSTRU - MENTATION	1 LS					1,304	35	45,600	3,600	25,200		74,400	14,900	1,500	40,600
HEAT TRACING	900 LF					900	35	31,500		1,400		32,900	6,600	100	39,600
SUBTOTAL MANIFOLD PIPING						6,834		256,400	33,600	83,400	10,000	403,400	80,700	5,600	489,700
AUGXILIARY SYSTEMS (INSTR. AIR, COOLING WATER)															
INSTRUMENT AIR COMPRESSOR	2 EA	60	400	5000		120	37.32	4,500	800		10,000	15,300	1,100	600	12,000
RECIRCULATION PUMP 50 GPM, 10 HP	1 EA	60	500	7000		60	37.32	2,200	500		7,000	9,700	500	400	10,000
CHILLER	1 EA	40	300	7000		40	37.32	1,500	300		7,000	8,800	400	400	9,600
MISC. ITEMS	1 LS	40	400	4000		40	37.32	1,500				5,900	1,200	200	7,300
PIPING AND INLINE INSTRUMENTATION AVG. DIA. 2.5"	2300 LF					2,690	38.78	104,300	12,500	36,600		153,400	30,700	2,200	186,600
ELECTRICAL INSTRUMENTATION	1 LS					777	35	27,200	3,700			35,100	7,000	300	42,400
SUBTOTAL AUX. SYSTEMS						3727		141,200	16,700	46,300	24,000	228,200	40,900	4,100	273,200
MONORAIL HOIST, 15 TON CAP.	3 EA	80	550	1500	30000	240	37.32	9,000	1,700	4,500	90,000	105,200	3,000	5,700	113,900

7.0 TECHNICAL ISSUES AND CONCERNS

The list of technical issues and concerns published as a part of the previous study is applicable to both the DAR and the IFR. A few additional items identified during the course of the present study are listed below.

1. Development of warmup strategies. External heating with properly selected subsets of heliostats as functions of the time of the day and year should be investigated for both the DAR and the IFR. Internal heating techniques, used exclusively or in combination with external heating, apply only to the IFR. The development of safe, automated warmup procedures is a complex problem, requiring special analytical techniques.

2. An extension of thermo-fluid and heat transfer investigations to include the effects of velocity gradients across the film due to rolling waves on local average and peak salt temperatures within the film. Significant effects on "particle residence times" have been reported by a number of investigators, including Blass and Wilke, at Reynolds numbers considerably below those encountered in film receivers. This phenomenon may affect salt thermal stability and control strategy.

3. Atmospheric particulate contamination of the salt, especially in arid countries with dust-laden atmospheres, like Egypt and Israel. This could significantly curtail the use of the DAR in these countries.

4. Salt/air interface transport phenomena in light of data reported by Dukler and others. Athough the effect on receiver efficiency appears to be minimal, an increased rate of CO2 and water vapor absorption by the salt film could have a significant impact on salt regeneration system design. (A DAR problem).

5. The development of IFR-specific structural support concepts, such as "pressurized" absorbers, and self-locking support structures.

6. The feasibility of direct heating of process fluids other than molten salt, with emphasis on desalination. (IFR advantage).

8.0 REFERENCES

1. Final Report, DAR Component Assessment and Design Studies, Solar Power Engineering Co., Inc. April, 1986

2. "Preliminary Design of a Solar Central Receiver for Site-Specific Repowering Application (Saguaro Power Plant)", -Cooperative Agreement DE-F-G03-825F-116752, September, 1983

3. "Arizona Public Service Company Utility Solar Central Receiver Study, Midterm Review" (in handout form), April 22-23, 1987

4. "Alternate Utility Team Utility Solar Central Receiver Study, Mid-Phase I Review Meeting" (in hadnout form), Part 2, April 22, 1987

5. Blass, E.: "Glass/Film Flow in Tubes", International Chemical Engineering, Vol. 19, No. 2, pp 183-194, April 1979

6. Wilke, W. : "Warmeubergang in Rieselfilme", VDI-Forschungsheft 490, 1962

7. Sandall, O.C., Hanna, O.T., and Wilson, C.L. : "Heat Transfer Across Turbulent Falling Liquid Films", AICH Symposium Series, Heat Transfer Niagara Falls, 1984

8. Dukler, A.E. : "Characterization, Effects and Modeling of the Wavy Gas-Liquid Interface", Progress in Heat and Mass Transfer, Vol. 6, pp 207-234, 1972

9. "Molten Salt Handbook", Martin Marietta Denver Aerospace, 1985

10. Abrams, M. : "The Solar Absorbtance of a Semi-Transparent Layer on an Opaque Substrate", Sandia Laboratories Report SAND75-8041, September 1985

11. "User's Manual for DELSOL 3", SAND86-8018, November 1986

12. "Final Report - Alternate Central Receiver Power System, Phase II", Martin Marietta Report MCR-81-1707, May, 1981

13. Fulford, G.D. : "The Flow of Liquids in Thin Films", Advances In Chemical Engineering, Vol. 5, pp 151-236, 1964

14. Siebers, D.L., Schwind, R.G., and Moffat, R.L. : "Experimental Mixed Convection Heat Transfer from a Large, Vertical Surface in Horizontal Flow", Sandia Report SAND83-8225, July, 1983

15. "Solar Central Receiver Utility Study, Guidelines, Ground Rules, and Trade Study Input Specifications", December 11, 1986

16. Hartog, J.P. : "Temperature Stresses in Flat Rectangular Plates and in Thin Cylindrical Tubes", Journal of the Franklin Institute, August, 1936, p 149

17. Kaiser Engineers : "Solar Central Receiver Cost Study, Sandia National Laboratories, Near Barstow, California", February, 1986

APPENDIX B

TABLES OF CALCULATIONS

This appendix contains several tables detailing calculations made in the course of this effort. Table B-1 lists the detailed receiver component costs for all three receivers, and Table B-2 shows the receiver subsystem costs. Both tables were developed from information provided by Bechtel [2]. The right-hand column indicates how the salt-in-tube receiver cost elements were scaled for the IFR and DAR.

Table B-1. Receiver Component Cost Analysis (in thousands of dollars)

Receiver Elements	S-I-T	DAR	IFR	Scaled By
Shop fabrication	$4,280	$1,593	$1,912	
Tube panels & attachments	$2,366	$911	$1,230	Weight of absorber materials (0.385=DAR, 0.52=IFR)
Headers caps & connective piping	$1,100	$275	$275	1/4 (no connective piping, smaller headers)
Cold & hot surge tanks	$104	$52	$52	1/2 (atm. pressure in cold tank)
Other shop costs	$710	$355	$355	1/2 (no tube welding or panel assembly)
Subcontracted Fabrication	$1,205	$558	$713	
Structural steel	$670	$258	$348	Weight of absorber materials (0.385=DAR, 0.52=IFR)
Panel support	$260	$100	$130	Weight of absorber materials (0.385=DAR, 0.52=IFR)
Insulation	$120	$71	$96	Area of absorber (DAR=0.593, IFR=.8)
Radiation shields	$80	$64	$64	Diameter of receiver (ratio=0.794)
Paint	$10	$0	$10	Not required for DAR, same for IFR
Freight	$65	$65	$65	
Auxiliary equipment	$1,480	$915	$915	
Heat tracing	$310	$155	$155	1/2 (no connective piping, smaller headers)
Valves	$380	$190	$190	1/2 (fewer and less critical valves)

Table B-1. Receiver Component Cost Analysis (in thousands of dollars) (Continued)

Receiver Elements	S-I-T		DAR		IFR		Scaled By
Instruments & controls	$440		$220		$220		1/2 (fewer sensors, simpler controls)
Crane	$250		$250		$250		
Electric & miscellaneous	$100		$100		$100		
Engineering & home office	$2,350		$2,350		$2,350		
Field erection	$3,100		$3,100		$3,100		
Total direct cost	$12,415		$8,516		$8,990		
Contingency (15%)	$1,862	$14,277	$1,277	$9,793	$1,349	$10,339	
G&A (7%)	$999	$15,277	$686	$10,478	$724	$11,062	
Fee (8%)	$1,222	$16,499	$838	$11,317	$885	$11,947	
		$16,499		$11,317		$11,947	
California sales tax (use 4.5% of total) (actually 6% on materials only)		$742		$509		$538	
Total capital cost		$17,241		$11,826		$12,485	

The costs for the receiver subsystems are shown in Table B-2. Note that the tower costs are different because the DAR and the IFR used the tower developed by PG&E for the lighter-weight sodium receiver. Another cost reduction for the IFR and DAR is for the cold salt pump. The cost of this item was decreased on the basis of an algorithm developed by Bechtel for early design study work. The algorithm accounts for the total head requirements on the pump and the thermal rating of the system. All the cold salt pump adjustments (cost and power) applied to the IFR were identical to the values used for the DAR.

Table B-3 shows the intermediate values used to calculate the performance of the IFR over a range of average fluxes. The average fluid temperature for the IFR was calculated from the salt temperature profile given in the SPECO report in Appendix A. The average salt-to-outer-surface conductance value was calculated from this same profile. Most of the other values were either taken directly or derived from the PG&E team Phase 1 viewgraphs [1].

Table B-2. Receiver Subsystem Cost Analysis (in thousands of dollars)

System Cost Categories	S-I-T	DAR	IFR	Notes
3.1 Receiver & auxiliaries	$17,241	$11,826	$12,485	Includes sales tax on materials (4.5% of total)
3.2 Tower	$5,999	$5,521	$5,521	Different tower structures
3.3 Piping	$4,031	$4,031	$4,031	
3.4 Mechanical equipment (pumps)	$1,439	$817	$817	Pump cost savings (56.8%)
3.5 IHX	$0	$0	$0	
3.6 Heat tracking & instrumentation	$11	$11	$11	
3.7 California sales tax	$153	$153	$153	
Subtotal	$28,874	$22,359	$23,018	
Contingency (15%)	$4,331	$3,354	$3,453	
Total receiver system cost	$33,205	$25,713	$26,471	
Difference in receiver system Costs		$7,492	$6,734	
Decrease as percentage of receiver cost		22.56%	20.28%	
Decrease as percentage of plant cost ($299,079)		2.51%	2.25%	

Table B-3. IFR Losses and Annual Performance

INPUT:	IFR		SIT	
Average T_{salt}	450°C		Absorber Area	1274°C
Absorptance	0.92		Average $T_{surface}$	557°C
Emittance	0.89		Emittance	0.89
Wall Conductance	6310 W/m^2-°C		T_{amb}	20°C
Annual Energy Incidence on Receiver	1,143,614 MWh/yr		Radiant Losses	144,818 MWh/yr
			Convectance Losses	48,272 MWh/yr
			Absorber Weight	10,243 lbs
			BOP Efficiency	0.3654

Average flux level (MW/m^2)	0.43	0.53	0.6	0.66	0.73
Total incident flux (MW)	536	542	546	549	553
Absorber area (m^2)	1247	1022	909	832	758
Average wall temperature (°C)	518	534	545	555	566
Radiation ratio	0.8052	0.7157	0.6731	0.6453	0.6203
Convection ratio	0.9078	0.7680	0.6980	0.6501	0.6042
Radiation losses (MWh/yr)	116,604	103,640	97,482	93,457	89,831
Convection losses (MWh/yr)	43,823	37,071	33,696	31,380	29,168
Reflection losses (MWh/yr)	91,489	91,489	91,489	91,489	91,489
Total losses (MWh/yr)	251,917	232,200	222,667	216,326	210,488
Annual energy delivered					
Thermal (MWh/yr)	891,697	911,414	920,947	927,288	933,126
Electric (MWh/yr)	328,921	336,126	339,609	341,926	344,059
Scaling ratios					
Area ratio	0.9787	0.8023	0.7139	0.6530	0.5946
Weight ratio	0.6355	0.5210	0.4636	0.4240	0.3861

SELECTED DISTRIBUTION LIST

Arizona Public Service Company
P.O. Box 21666
Phoenix, AZ 85036
Mr. Eric Weber

Babcock and Wilcox
91 Stirling Ave.
Barberton, OH 44203
Mr. Dan Young

Battelle Pacific NW Laboratory
P.O. Box 999
Richland, WA 99352
Mr. Tom A. Williams

Bechtel Corporation
P.O. Box 3965
San Francisco, CA 94119
Mr. Pascal de Laquil

Black and Veatch Consulting
Engineers
1500 Meadow Lake Parkway
Kansas City, MO 64114
Dr. Charles Grosskreutz

Department of Energy/HQ
Forrestal Building
1000 Independence Ave., SW
Washington, DC 20585
Dr. H. Coleman
Mr. S. Gronich
Mr. C. Mangold
Mr. M. Scheve
Mr. Frank Wilkins

DFVLR
German Aerospace Research
Establishment
Linder Höhe
D-5000 Köln 90
West Germany
Ingo Susemihl, Dipl.-Ing.

Foster Wheeler Solar Development
Corp.
12 Peach Tree Hill Road
Livingston, NJ 07070
Mr. S. F. Wu

Luz International Limited
924 Westwood Blvd.
Los Angeles CA 90024
Dr. David W. Kearney

Martin Marietta
P.O. Box 179
Denver, CO 80201
Mr. Tom Tracey

Pacific Gas and Electric Company
3400 Crow Canyon Rd.
San Ramon, CA 94583
Mr. Tom Hillesland

Plataforma Solar de Almeria
Apartado 22
04200 Tabernas (Almeria)
SPAIN
Dr. Felipe Rosa

Sandia National Laboratories
Solar Energy Department 6220
P.O. Box 5800
Albuquerque, NM 87185
Mr. John Otts
Mr. James Leonard
Mr. John Holmes
Mr. Craig Tyner

Solar Energy Research Institute
1617 Cole Blvd.
Golden, CO 80401
Mr. B. P. Gupta
Dr. Robert A. Stokes